2018

Targeting the CD4 Binding Site of HIV

Lotta von Boehmer

TARGETING THE CD4 BINDING SITE OF HIV

A Thesis Presented to the Faculty of

The Rockefeller University

in Partial Fulfillment of the Requirements for

the degree of Doctor of Philosophy

by

Lotta von Boehmer

June 2018

TARGETING THE CD4 BINDING SITE OF HIV

Lotta von Boehmer, Ph.D., M.D.

The Rockefeller University 2018

The immunologic obstacles to develop a broadly neutralizing antibody (bNAb) against HIV by vaccine mandate for methodical testing in order to understand and direct the immune response. A mouse model with the predicted human heavy chain variable domain of a bNAb precursor or mature version introduced into the mouse heavy chain immunoglobulin locus proved to be very useful. The immunoglobulin heavy-chain of the predicted germline (GLVH) or mature mutated (MuVH) version of 3BNC60 was knocked into the JH4 locus in mice. 3BNC60 is a bNAb that targets the CD4 binding site (CD4bs) of HIV-1[1,2] and belongs to the IgHV1-2 class of broadly neutralizing CD4bs antibodies[3]. In the first part of my thesis I will describe the evolution of the HIV-1 antibody response in GLVH and MuVH mice upon immunization. We immunized the mice with antigens designed to bind to the predicted unmutated precursor of 3BNC60 or with BG505 SOSIP trimers that resemble the native HIV-1 Env. Immunogens specifically designed to activate B cells bearing germline antibodies initiate immune responses, but they do not elicit bNAbs. In contrast, native-like Env trimers fail to activate B cells expressing germline antibodies but elicit bNAbs by selecting for a restricted group of light chains bearing specific somatic mutations that enhance neutralizing activity. The data suggest that vaccination to elicit broad anti-HIV-1 antibodies will require immunization with a succession of related immunogens.

Although CD4bs bNAbs are attractive candidates for immunogen design, their

features, such as a high degree of somatic hypermutation and a short CDRL3 in combination with our data in 3BNC60 knock-in mice suggest that they might be difficult to elicit through vaccination. In the second part I will describe IOMA, a new class of CD4-mimetic bNAb derived from the VH1-2 germline but with a normal-length CDRL3 and fewer somatic hypermutations than other bNAbs of its class. We defined IOMA's complete epitope, by using crystal structures of a natively glycosylated Env trimer. Analysis of the native glycan shield on HIV-1 Env allowed us to provide what is, to our knowledge, the first full description of the interplay between heterogeneous untrimmed high-mannose and complex-type N-glycans within the CD4bs and of a natively glycosylated trimer.

DEDICATION

For their unconditional support and love I dedicate this thesis to my parents.

ACKNOWLEDGMENTS

First, I would like to thank my advisor Michel Nussenzweig. Without his clear guidance and continuous support the work in this thesis would not have been possible. My experience in Michel's lab has helped me grow and I am truly grateful for the mentorship.

I owe a great deal of thanks to many people: Klara Velinzon and Neena Thomas for help with FACS single cell sorting; Anna Gazumyan, Cassie Liu and Jovana Golijanin for antibody cloning; Thiago Oliveira for bioinformatics analyses. Natalie Freund, Hugo Moquet, Johannes Scheid, Marina Caskey, Pia Dosenovic, Florian Klein, Philipp Rommel, Qiao Wang, Yotam Bar-On and Joshua Horwitz for discussions and friendship. Pamela Bjoerkman for support and the great collaboration on IOMA together with Harry Gristick and Anthony West. Davide Robbiani and Mila Jankovic for advice and discussion; Zoran Jankovic for laboratory support; Virginia Menendez, Jennifer McQuillan and Adriana Barillas-Batarse for administrative assistance; Mukul Mathur, Alyssa Luong and Mei-Ki Chan for excellent grant submission support. The Nussenzweig lab as a whole has been an immensely enjoyable place to work over the last few years, and I have all of the members, past and present, to thank for this. Many thanks to the Clinical Scholars Program, in particular Barry Coller, Sarah Schlesinger and Michelle Romanik, and the Rockefeller Dean's office for their wonderful support, guidance and advice over the years. And finally, Mike Seaman for agreeing to travel from Boston to be the external examiner on my thesis committee; Sohail Tavazoie, Sarah Schlesinger and Gabriel Victora for continuous support, guidance and service on my thesis committee.

TABLE OF CONTENTS

LIST OF FIGURES

CHAPTER 1: INTRODUCTION

1.1 HIV-1

78 million people have become infected with HIV-1 since the start of the epidemic. In 2015, 36.7 million people lived with HIV-1. Education, identification and treatment of infected patients with retroviral drugs have been effective at curtailing the epidemic, but declines in the rate of new infections have plateaued: every year since 2010, around 1.9 million adults have become newly infected with HIV-1. Not only that, but in 2015, 1.1 million people died from AIDS-related causes worldwide. One reason that such high rates of new infections and AIDS-related deaths continue to occur globally, is that only 18.2 million people living with HIV-1 have access to therapy (statistics from unaids.org and CDC HIV surveillance report).

Under status quo interventions, a median of 49 million incident cases are predicted globally from 2015 to 2035. With the 2020 introduction of a 50%-efficacy vaccine gradually scaled up to 70% coverage it was estimated to avert 25-31 million of these new infections[4-6]. The added benefit of prevention through vaccination motivates scientists world wide. Despite a concerted effort since 25-30 years, testing of candidate vaccines in trials has been disappointing[7-11], with only one trial showing any degree of vaccine efficacy[12,13].

1.2 VACCINES

As the immune system starts to mature, it is exposed to many pathogenic viruses, bacteria, fungi and parasites. Without good nutrition, hygiene and comprehensive vaccination, high mortality rates savage infants and young children. Infections induce immune responses involving both the innate and adaptive immunity with more than 1600 genes orchestrating these immune

responses[14]. The adaptive immune system antibody-tags pathogens for further processing, CD4+ T cells suppress or regulate immune responses and CD8+ cytotoxic T cells recognize and eliminate infected cells. Such responses usually control and eliminate viruses effectively and the person is left with protective immunological memory against subsequent infections with the same virus. Vaccines imitate this successful process of nature. Edward Jenner, an english physician and scientist, wondered if cowpox, a mild infection that caused sores on the milkmaids' hands for a few days, protected these maids from smallpox. He was the first to test the theory by exposing a young boy to cowpox, then later exposing him to smallpox: the cowpox virus did make the boy immune to the similar, but far more deadly smallpox virus. With this experiment Jenner pioneered the smallpox vaccine, the world's first vaccine. Given in an appropriate formulation and dose before exposure, vaccines induce immune responses that mimic the response to natural infections and protect recipients from the development of clinically apparent disease when they are exposed to them[15].

1.3 HIV-1 VACCINE CHALLENGE

The situation is more complex with HIV-1 infection, the natural immune response once primary infection is established, fails to eradicate or control the virus in most patients. Multiple reasons explain this failure: HIV-1 targets the CD4+ T cells, hindering thereby the orchestration of an effective immune response, HIV-1 escapes the adaptive immune system by mutating and recombining the targets for specific B and T cell receptors, in particular it rapidly mutates Env, the trimeric envelope glycoprotein present in low numbers on its surface and the main antibody target, HIV-1 shields itself with self-glycans that are attached during particle synthesis in host cells. In addition to all of the above, once inside a CD4+ T cell, HIV integrates into the host DNA[16], hiding from the immune system and entering a latent state for years. Combinations of ART were shown to reduce plasma virus levels to

below the limit of detection[17-19], but it rapidly became clear that the latent reservoir of HIV-1 in resting CD4+ T cells is not affected by ART[20]. The initiation of ART in infected individuals as early as 10 days after the onset of symptoms of primary HIV-1 infection does not prevent generation of latently infected, resting CD4+ T cells[21]. Studies from non-human primates suggest the reservoir is established as early as 24-72 hours after intravenous infection[22,23], and 36-72 hours after vaginal or rectal infection[24,25]. Recently, it was shown that HIV-infected quiescent CD4+ T cells have a particular gene expression signature and that CD32a+ lymphocytes may harbor the elusive HIV-1 reservoir, this knowledge may facilitate the targeting and elimination of this reservoir[26].

1.4 ANTIBODIES DURING NATURAL HIV-1 INFECTION

HIV-1 transmission results most commonly from virus exposure at mucosal surfaces and induces a vigorous but ineffective immune response[27]. A single virion is responsible for HIV-1 transmission in approximately 80% of heterosexuals, in 60% of men who have sex with men and 40% of injection-drug users[28-33]. For practical reasons, it has been impossible to characterize HIV-1 at the moment of transmission, yet it is this virus the immune system must target. The earliest pressure on the virus is driven by the CD8+ T cells[34], resulting in complete turnover of the virus pool within the first few weeks of infection[35]. The development of antibody responses follows a pattern, with antibodies directed to the HIV-1 Env glycoprotein 41 (gp41) subunit, and then by the development of Env glycoprotein 120 (gp120)-binding antibodies[13,36,37]. For clade B patients, the initial gp120 target is the variable loop 3 (V3). These early antibody responses do not neutralize, but they are closely followed by weakly tier 1 HIV-1 neutralizing V3 antibodies. IgG antibodies to Gag appear around the same time as antibodies directed against the HIV-1 Env and after 7 weeks antibodies to p31 (integrase) are elicited[13,38]. A large proportion

(~20-25%) of HIV-1-infected patients develop cross-reactive neutralizing antibodies but broadly neutralizing antibodies are not routinely made in HIV-1 infection (1%), and when they are made, they arise late[38].

1.5 BROAD NEUTRALIZING ANTIBODIES

Longitudinal studies of HIV-1 infected patients have allowed to associate the development of neutralization breadth with high viral load[39-41] and time since infection[42]. The frequency of bNAbs in individuals taking or not taking ART was similar[43], although not all individuals taking ART were entirely suppressed. With a few exceptions[44], bNAbs do not develop until at least 2 years after HIV-1 infection and common demographic characteristics do not appear to influence the development[13,41], but multiple studies have demonstrated that virus neutralization is a driver of both virus and antibody diversity[44-48]. In summary, multiple factors contribute to the development of breadth in HIV-1-infected individuals but it is not entirely clear what is needed for bNAb development.

The first generation of bNAbs to HIV-1 (b12, 2G12, 2F5, and 4E10) were isolated by phage display or human hybridoma electrofusion, selected for binding to Env peptides or monomeric proteins. They have limited breadth and/or potency[49-52]. High-throughput neutralization assays and standardized HIV-1 categorization directed the efforts of bNAb isolation to HIV patients with exceptionally potent and broad sera[53,54]. Antibodies targeting novel epitopes and/or possessing greater breadth and potency have been identified by our laboratory using antigen labeled, flow cytometry-single cell sorted B cells and by others using cultured memory B cells[55,1,56-62]. These broad HIV-1 neutralizing antibodies have unusual characteristics, they have a high degree of somatic mutations[63-67], they have nucleotide insertions and/or deletions, they have very long heavy-chain complementarity determining region 3 (HCDR3) loops and can be autoreactive[55,68]. No reported bNAb lacks all

characteristics. Autoreactivity, long HCDR3 loops, and high levels of somatic hypermutation is a main pathway for B cells to be deleted by central and peripheral tolerance controls[69-73]. The co-evolution of bNAbs with HIV-1 in the host through multiple rounds of HIV-1 escape from antibody pressure[47,74-76] might explain the ability to develop antibodies with these unusual characteristics. For vaccine development, these unusual bNAb traits pose daunting immunologic obstacles, however, it seems a worthwhile goal since passive immunization with bNAbs has been shown to block infections of simian immunodeficiency virus and simian-HIV-1 in nonhuman primates and passive infusion with bNAbs leads to rapid, although transient, suppression of viral load in chronically infected macaques and humans (reviewed in[77,78]).

1.6 VULNERABLE HIV-1 SITES

Occasionally, individual monoclonal antibodies can account for the serum activity[57,79], but breadth and potency are most frequently attributed to a combination of unrelated antibodies that target different sites of vulnerability on the Env spike[55,61,76,80]. The targets of the bNAbs can be divided into the following major groups: (1) the N160 glycan-dependent site associated with the V1/V2 loops, (2) the N332 glycan-dependent site at the base of the V3 loop, (3) the membrane-proximal external region (MPER) on gp41 and (4) the gp120-gp41 interface and (5) the CD4-binding site (CD4bs).

(1) The N160 glycan-V1/V2 site is targeted by the antibodies PG9 and PG16, CH01-04, PGT141-145, CAP256.09 and PGDM1400[56,57,60,74,81,82]. Structural analyses showed that these antibodies penetrate the glycan shield with an exceptionally long anionic CDRH3 that contacts a β-strand on gp120. These bNAbs are sensitive to natural glycan heterogeneity, which means a fraction of virions may be resistant to neutralization because they contain glycoforms that are not recognized by the antibodies, resulting in incomplete neutralization curves[83].

(2) The N332 glycan-V3 loop site is targeted by the PGT121/4-, PGT128-, PGT135- and 10-1074 bNAbs[57,68,84]. These high-mannose patch bNAbs do not appear to share particular genetic traits required for binding[57,85]. By comparing structural information generated for different families within this class, it was shown that the N332/GDIR epitope is accessed from a variety of angles[85,86]. At least two antibodies of this class block infection by interfering with CD4 binding[87].

(3) 10E8 targets the MPER in gp41. This antibody recognizes an α helix, and unlike 2F5 and 4E10, which were less-potent first-generation antibodies targeting a closely related site, 10E8 is reported not to be auto- or phospholipid-reactive[88].

(4) The fourth class of bNAb is highly divergent and targets the gp120-gp41 interface (8ANC195, PGT151, VRC34, 35O22, and 3BC315). The bNAbs have been isolated in rapid succession over the last few years[59,89-91], and some previously identified bNAbs have been shown to bind to this region[80,92,93]. The members of the class target non-overlapping epitopes and many do not compete with one another[90].

(5) The CD4 binding site class of antibodies is the broadest known class so far. It consists of two subclasses that effectively neutralize HIV-1 through CD4 mimicry, those derived from the VH1-2 germline, which include the well-characterized 3BNC117, 3BNC60 and VRC01 antibodies[1,57], and those derived from VH1-46, like 8ANC131. The accessibility to the conserved CD4bs on gp120 is restricted by surrounding glycans[94-99]. Although CD4bs bNAbs are attractive candidates for immunogen design, their features, such as a high degree of somatic hypermutation and a short (five-residue) light chain complementarity-determining region 3 (CDRL3) (found in only 1% of human light chains) suggest that they might be difficult to elicit through vaccination.

1.7 A VACCINE MODEL

The immunologic obstacles to develop a bNAb by vaccine mandate for methodical testing in order to dissect the immune response. A mouse model with the predicted human heavy chain variable domain of a bNAb precursor or mature version introduced into the mouse heavy chain immunoglobulin locus proved to be very useful. Our laboratory knocked the immunoglobulin heavy-chain of the predicted germline (GLVH) or mature mutated (MuVH) version of 3BNC60 in mice. 3BNC60 is a bNAb that targets the CD4bs of HIV-1[1,2] and belongs to the IgHV1-2 class[3]. In this mouse the human variable bNAb heavy chain domain forms antibodies using the mouse constant region and mouse light chains. These mice have a restricted B cell repertoire because the heavy chain is fixed. Nevertheless, the repertoire remains relatively diverse because the antibody light chain is produced by random VJ recombination in developing B cells. Thus, only a small fraction of the B cells carry heavy and light chains that combine to produce antibodies able to bind to the HIV-1 Env (see below). Immunization of GLVH mice affords the opportunity to evaluate antigens for their ability to select B cells expressing light chains that show features that could support bNAb evolution. In contrast, MuVH mice represent a synthetic intermediate because the human heavy chain carries all of the required mutations, but the mouse light chain is germline. To track the evolution of the HIV-1 antibody response in GLVH and MuVH mice, we immunized them with antigens designed to bind to the predicted unmutated precursor of 3BNC60 or with BG505 SOSIP trimers that resemble the native HIV-1 Env.

1.8 AN ALTERNATIVE BROADLY NEUTRALIZING ANTIBODY

Although CD4bs bNAbs are attractive candidates for immunogen design, their features, such as a high degree of somatic hypermutation and a short CDRL3 suggest that they might be difficult to elicit through vaccination. In the second part I will describe IOMA, a new class of CD4-mimetic bNAb derived from the VH1-2 germline, but with a normal-length CDRL3 and fewer somatic hypermutations than other bNAbs of its class. We defined IOMA's complete epitope, by using crystal structures of a natively glycosylated Env trimer. Analysis of the native glycan shield on HIV-1 Env allowed us to provide what is, to our knowledge, the first full description of the interplay between heterogeneous untrimmed high-mannose and complex-type N-glycans within the CD4bs and of a natively glycosylated Env trimer.

CHAPTER 2: IMMUNIZATION FOR HIV-1 BROADLY NEUTRALIZING ANTIBODIES

2.1 THE MODEL: 3BNC60 KNOCK-IN MICE

Natalia Freund and Alex Gitlin in the laboratory created mouse models knocking in the 3BNC60 CD4 binding site antibody previously isolated by Johannes Scheid in the laboratory[1]. To explore the obstacles encountered for the induction of bNAbs with HIV vaccination, we immunized the immunoglobulin (Ig) heavy-chain knock-in (KI) mice expressing the predicted germline (GLVH) or mature mutated (MuVH) version of 3BNC60 heavy chain (Figure 1).

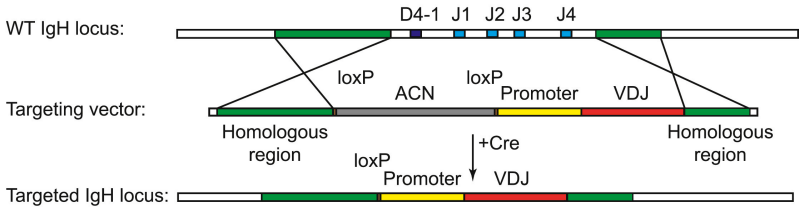

Figure 1: Schematic figure of the targeting strategy used for the generation of VDJ KI mice. Targeting vector-encoded arms of homology to the C57Bl6 wild-type (WT) mouse IgH locus are indicated in green; the neo cassette (ACN) is indicated in gray flanked by loxP sites indicated in brown. The promoter and the human heavy chain VDJ sequences are indicated in yellow and red, respectively.

GLVH has all of the heavy chain residues reverted, except for the CDRH3. CDRH3 harbors the V-D and D-J junctions, where imprecision in the site of joining allows exonucleolytic loss as well as palindromic gain of the terminal V, D and J germline sequences thus preventing us from predicting the germline VDJ with certainty. Both heavy chain knock-in strains showed near normal frequencies of immature and recirculating B cells in the bone marrow

and of mature B cell populations in the spleen.

To determine the frequency of naive B cells that bind to Env-based antigens in the KI mice, we stained splenocytes with an improved version (eOD-GT8) of the previously described immunogen eOD-GT6, an engineered outer domain of gp120 designed to bind to both germline and mature versions of 3BNC60 and other VH1-2-class antibodies (see below and[100]). The average number of naive B cells that bind to eOD-GT8 in GLVH and MuVH mice (0.08% and 0.13%, respectively) was similar to that found in wild-type C57Bl6 mice (0.05%) indicating that these cells are rare and found at frequencies similar to those in wild-type C57Bl6 mice (Figure 2A–B).

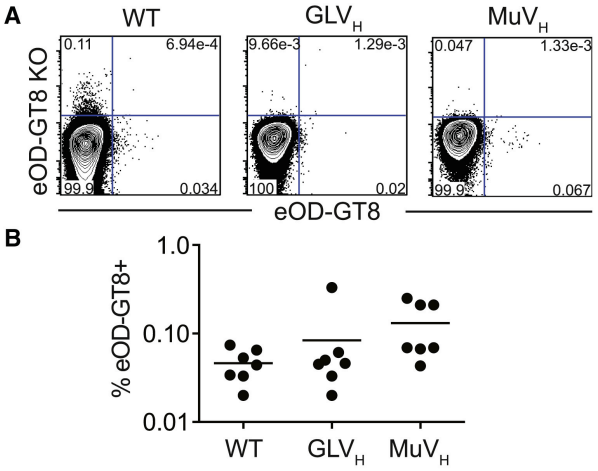

Figure 2A: Representative FACS plots show binding of eOD-GT8 and eOD-GT8 CD4bs knock-out (KO) proteins by mature naive B cells in naive wild-type C57Bl6 (WT), GLVH, and MuVH mice. B: Graph shows frequency of eOD-GT8-binding B cells in naive WT, GLVH, and MuVH mice. Each dot represents one mouse. Lines indicate mean of the group.

To examine the naïve and memory antibody repertoire in these mice I initially used published protocols for mouse plasma cell sequencing[101], which proved to be very inefficient (4% amplification) for the analysis of naïve and memory

B cells. After designing a protocol, amplification efficiency reached 60-90%[102], which allowed us to isolate single cells by flow cytometry and sequence their Ig genes. As expected, the heavy chain was always the product of the respective knock-in allele and the mouse light chain sequences were less diverse than in wild-type C57Bl6 B cells (51/59, 24/44 and 33/63 unique sequences for wild-type C57Bl6, GLVH and MuVH respectively; Figure 3A). Consistent with the rare occurrence of antigen-binding cells in the naive knock-in mice (Figure 2A and B), none of the mouse light chains showed the 5-residue CDRL3 signature typical of authentic 3BNC60 or of other VH1-2-class antibodies (Figure 3B).

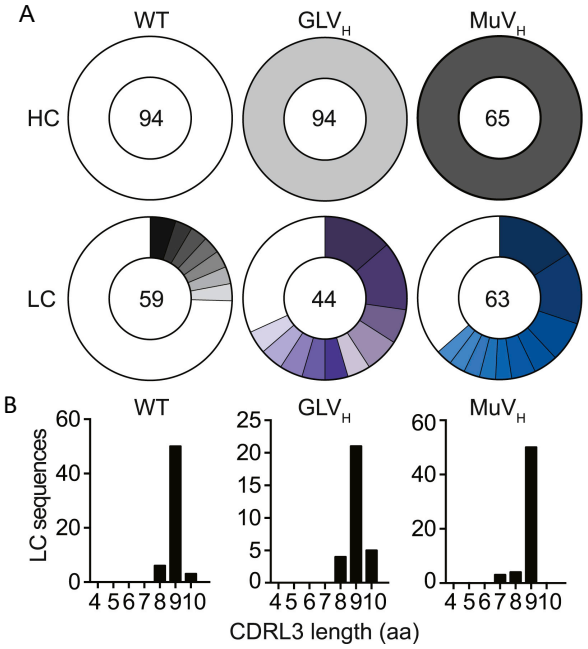

Figure 3A: Pie charts show heavy- (HC) and light-chain (LC) sequences cloned from purified single-cell sorted B cells from naive mice. The number in the center of the pie chart is the number of sequences analyzed, each colored slice represents one clone (identical V gene and CDRL3), and its size is proportional to the size of the clone. White indicates unique sequences. B: CDRL3 aa lengths from LCs in (A).

2.2 IMMUNE RESPONSES IN 3BNC60 GLVH KNOCK-IN MICE

Like most other potent bNAbs, reversion of the somatic mutations in the 3BNC60 antibody to the predicted germline antibody results in complete loss of affinity and neutralizing activity for all recombinant HIV-1 Env proteins and viruses tested[1,68,100,103-105]. To determine whether naive GLVH B cells can be stimulated with antigens that are specifically engineered to activate cells expressing germline VH1-2-class antibodies, we immunized these mice and wild-type C57Bl6 controls with eOD-GT8 60mers or with multimerized 426c.TM4ΔV1-3 ([106] and see methods). 426c.TM4ΔV1-3 is a 426c env -derived construct that was optimized to be recognized by most inferred germline VH1-2-class antibodies. Immunization produced a robust antibody response in wild-type C57Bl6 and GLVH mice after one or two immunizations (Figure 4A and B).

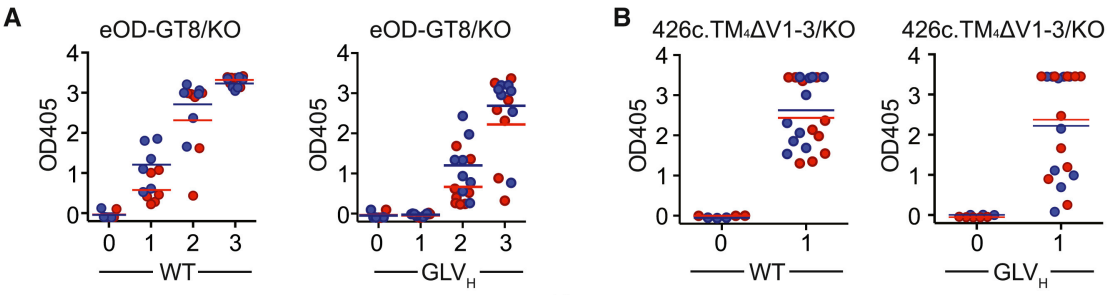

Figure 4A: Graphs show ELISA results of serum (1/900 dilution) for individual mice against eOD-GT8 (blue) and eOD-GT8 CD4bs knock-out (KO, red) from wild-type C57Bl6 (WT) and GLVH mice. Naive serum (0) and serum after one, two, or three (1, 2 or 3) immunizations with eOD-GT8 60-mer. B: Graphs show ELISA results of serum (1/900 dilution) for individual mice against 426c.TM4ΔV1-3 (blue) or 426c.TM4ΔV1-3 CD4bs knock-out (KO, red) from wild-type C57Bl6 (WT) and GLVH mice. Naive serum (0) and serum after one (1) immunization with multimerized 426c.TM4ΔV1-3.

Although the response was not restricted to the CD4bs, as determined by ELISA, sera from the eOD-GT8 60mer-immunized mice showed some preference for the wild-type vs. a control eOD-GT8 CD4bs knock-out protein (Figure 4A). Finally, none of the sera from the eOD-GT8 60mer-immunized mice showed cross-reactivity to a native-like BG505 SOSIP[87,107] or a YU2 gp140 foldon trimer (YU2 gp140-F)[108] (Figure 5).

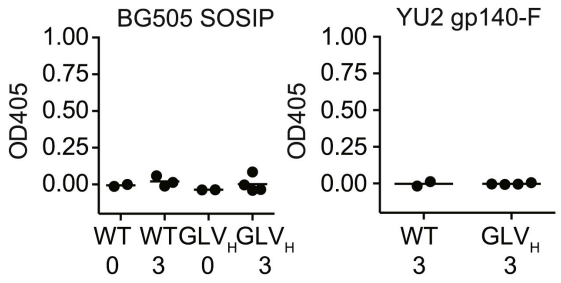

Figure 5: Graphs show ELISA results of serum (1/300 dilution) for individual mice against BG505 SOSIP and YU2gp140-F in naive mice (0) or after three (3) immunizations with eOD-GT8 60-mer.

eOD-GT8-binding IgG+ B cells are rare in GLVH naive mice but increase to 5.8% on average after immunization. A fraction of these cells appeared to express CD4bs-specific antibodies as measured by flow cytometry. To further characterize the B cell responses to eOD-GT8 60mers in GLVH mice, we sorted single cells that bound to eOD-GT8, but not eOD-GT8 CD4bs knock-out, and cloned their antibody genes with a protocol I developed for high throughput cloning of mouse antibodies[102](Figure 6).

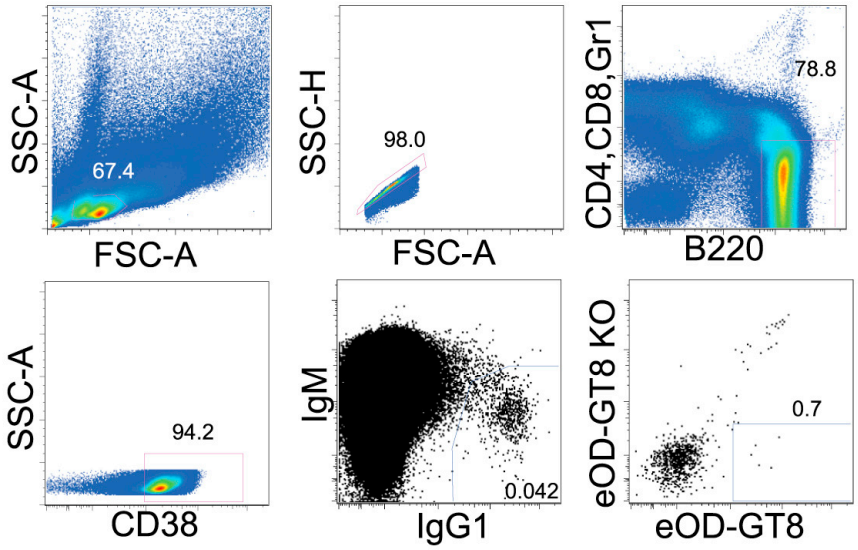

Figure 6: Gating strategy for single cell sorting of eOD-GT8 CD4bs-specific memory B cells in eOD-GT8 60-mer-immunized GLVH mice.

After sorting eOD-GT8 CD4bs-specific memory B cells 71 light and 55 heavy chain sequences were obtained from 4 mice. As expected, all of the heavy chains were GLVH. The 71 light chains include 8 clones ranging in size from 2–13 clonal members, one of which appeared in more than one mouse. In addition, there were 13 cells that carried unique sequences (Figure 7A, C). The CDR3 length of the light chains was similar to the lengths in wild-type C57Bl6 mice, with only one of the expanded clones showing the 5 residue CDRL3 signature typical of 3BNC60 and related antibodies (Figure 7B, D).

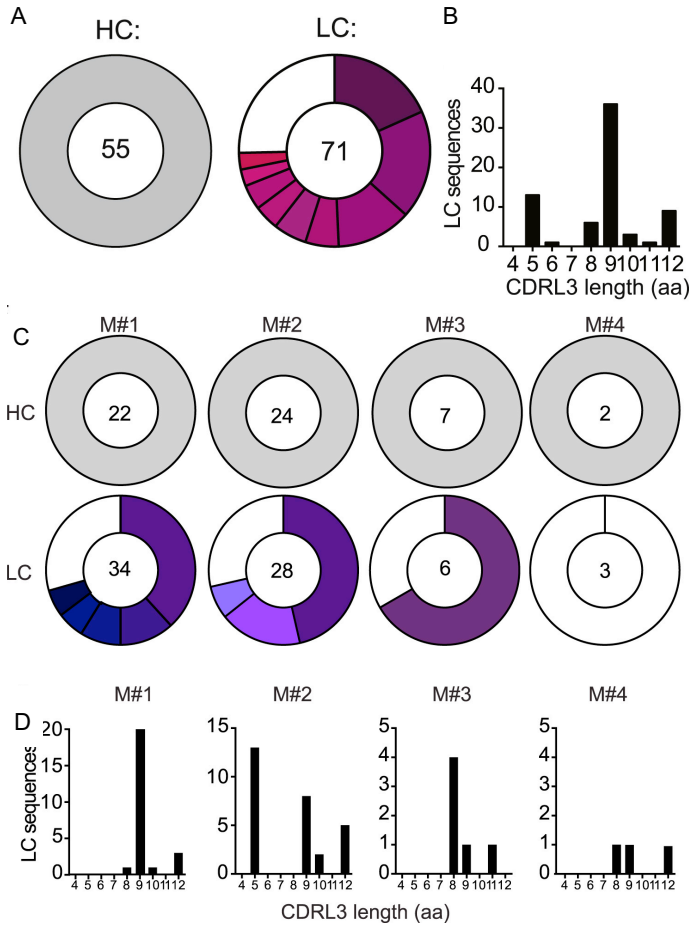

Figure 7A: Heavy- (HC) and light-chain (LC) sequences from single antigen-binding B cells isolated from four eOD-GT8 60-mer-immunized GLVH mice. Pie charts as in Figure 1A. A clone is defined by identical V gene and similar CDRL3. B: CDRL3 aa lengths from LCs in (A). C: Heavy- (HC) and light-chain (LC) sequences of sorted B cells from individual eOD-GT8 60-mer-immunized GLVH mice (M# 1, 2, 3 and 4), organized in clones. The number in the center of each pie chart is the number of sequences analyzed; each clone is represented by one slice and its size is proportional to the size of the clone; colors indicate clones (identical V gene and similar CDRL3) and white indicates unique sequences. D: CDRL3 aa lengths of cloned LC sequences in (C).

Out of 20 antibodies cloned from B cells expressing antibodies that bound to eOD-GT8 but not eOD-GT8 CD4bs knock-out by FACS, 7 were CD4bs specific as measured by ELISA (Figure 8).

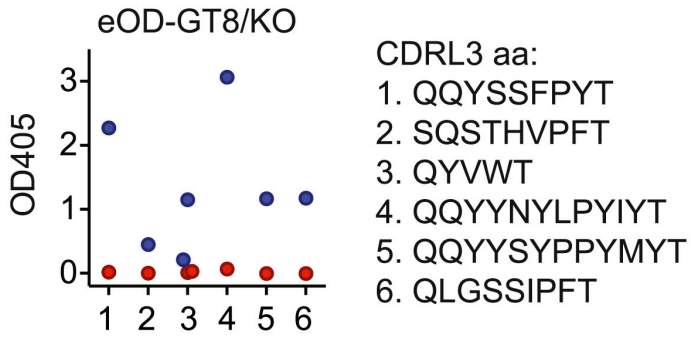

Figure 8: Graph shows ELISA results for monoclonal antibodies (5 µg/ml) cloned from eOD-GT8 60-mer-immunized GLVH mice against eOD-GT8 (blue) and eOD-GT8 CD4bs knock-out (KO, red).

However, none of the 17 monoclonal antibodies analyzed, neutralized any of the tier 1 and 2 viruses tested[2]. We conclude that the eOD-GT8 60mer, an antigen designed to activate B cells expressing germline 3BNC60 antibody, elicits B cell responses in mice that carry germline knock-in antibody heavy chains including B cells expressing antibody light chains with 5-residue CDRL3s, but these antibodies do not neutralize HIV-1.

To determine whether GLVH B cells can respond to a more native appearing HIV-1 antigen in vivo, we immunized these mice and wild-type C57Bl6 mice with BG505 SOSIP[87,107] or YU2 SOSIP[108]. Wild-type C57Bl6 mice developed detectable antibody responses as measured by ELISA. In contrast, GLVH mice failed to respond to these antigens (Figure 9). We conclude that naive B cells expressing GLVH paired with a heterogeneous group of mouse light chains fail to mount significant immune responses to BG505 SOSIP or YU2 SOSIP.

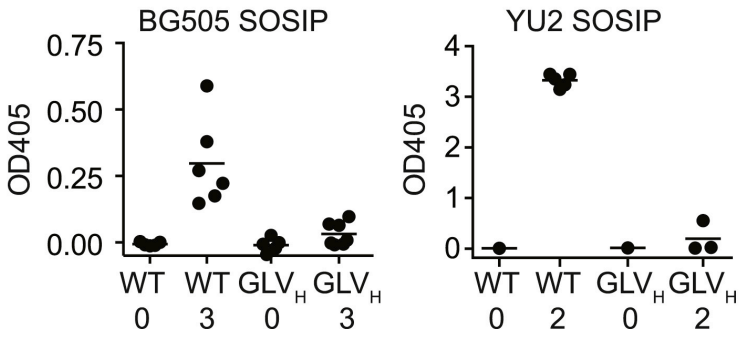

Figure 9: Graphs show ELISA results of serum (1/300 dilution) for individual mice against BG505 SOSIP or YU2 SOSIP in wild-type C57Bl6 (WT) and GLVH mice after immunization with BG505 SOSIP or YU2 SOSIP, respectively. Naive serum (0) and serum after two (2) or three (3) immunizations.

2.3 IMMUNE RESPONSES IN 3BNC60 MuVH KNOCK-IN MICE

Serum from naive MuVH mice has no detectable HIV-1 Env-binding activity in ELISA or neutralizing activity in TZM-bl assays[2]. To determine whether anti-HIV-1 antibodies can be elicited in these mice they were immunized three times, with eOD-GT8 60mers or BG505 SOSIP. The eOD-GT8 60mer immunization produced strong serologic responses in MuVH mice but the sera were not cross-reactive against other HIV-1 proteins such as 2cc-core (an engineered gp120[109]) or YU2 gp140-F[108], and a fraction of the mice showed CD4bs specificity as measured by ELISA on eOD-GT8 and eOD-GT8 CD4bs knock-out (Figure 10A). MuVH mice also developed strong serologic responses to BG505 SOSIP, but in contrast to eOD-GT8 immunization, there was serologic cross-reactivity to 2cc core, as well as YU2 gp140-F. Moreover, a significant fraction of the response was CD4bs specific as determined by ELISA against YU2 gp140-F and a YU2 gp140-F CD4bs knock-out mutant protein (Figure 10B).

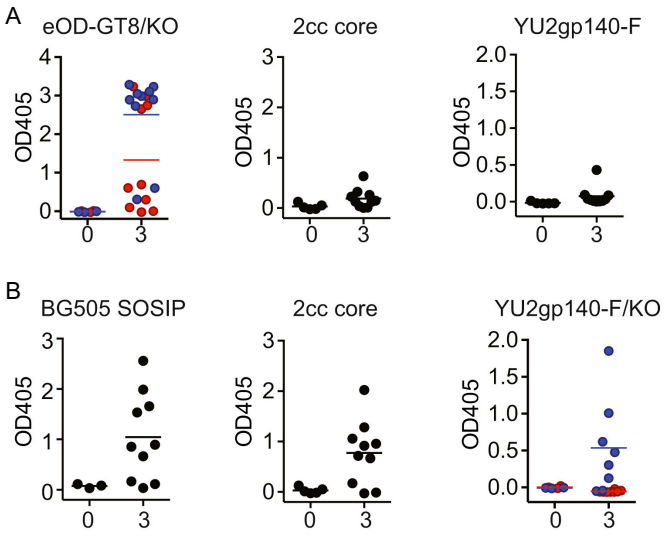

Figure 10A: Graphs show ELISA results of serum (1/300 dilution) for individual mice against eOD-GT8 (blue) and eOD-GT8 CD4bs knock-out (KO, red), 2cc core, and YU2 gp140-F. Naive serum (0) and serum after three (3) immunizations with eOD-GT8 60-mer. B: As in (A) but after BG505 SOSIP-immunization. ELISA against BG505 SOSIP, 2cc core, and YU2 gp140-F (blue) and YU2 gp140-F CD4bs knock-out (KO, red). Lines indicate mean of the group and the colors of the lines correlate to the colors of the dots.

To determine whether MuVH mice develop HIV-1 neutralizing responses we assayed mouse serum on a panel of 9 HIV-1 viruses (8 tier 2, and 1 tier 1) in TZMbl-assays[110]. We found that the eOD-GT8 60mer-immunized MuVH mice only showed modest levels of activity mainly against tier 2 Clade D (T247-23) and A (62357.14.D3.3489) viruses that lack glycosylation at position 276 (Genebank entry ACD63071 and ABY50658.1, respectively) (Figure 11). In contrast, all seven out of ten BG505 SOSIP-immunized MuVH mice that showed a robust response to BG505 SOSIP in ELISA, developed strong neutralizing responses against the autologous Clade A virus. In addition, high levels of neutralization were also evident against T247-23, and 62357.14.D3.3489, and more modest levels of neutralization were seen against three other clade A tier 2 viruses. Finally, four of the seven also

showed a low level of neutralizing activity against the clade B tier 2 strain YU2.DG (Figure 11). Thus, BG505 SOSIP trimers elicit potent responses with some cross-clade breadth in MuVH mice but eOD-GT8 60mer does not.

		Tier:	1	2								
		Clade:	B	A	D	A	A	A	A	A	B	B
		Virus:	MuLV	HxBC2.DG	BG505/T332N	T247-23	62357.14 D3.3489	Q842.d12	0330.v4.c3	3365.v2.c30	Q769_D22	REJO 4541.67	YU2.DG
		M#:											
Naive	20		<50	<50	<50	<50	<50	<50	<50	<50	<50	<50	<50
Naive	21		<50	<50	<50	<50	<50	<50	<50	<50	<50	<50	<50
Naive	22		<50	<50	<50	<50	<50	<50	<50	<50	<50	<50	<50
eOD-GT8 60mer-immunized	4		<50	<50	<50	521	212	<50	<50	<50	<50	<50	<50
eOD-GT8 60mer-immunized	5		100	<50	76	254	144	105	98	110	78	101	66
eOD-GT8 60mer-immunized	6		<50	<50	<50	<50	<50	<50	<50	<50	<50	<50	<50
eOD-GT8 60mer-immunized	7		<50	<50	<50	291	<50	<50	<50	<50	<50	<50	<50
eOD-GT8 60mer-immunized	8		<50	<50	<50	1,371	<50	<50	<50	<50	<50	<50	<50
eOD-GT8 60mer-immunized	9		<50	<50	<50	2,225	<50	<50	76	<50	<50	<50	<50
eOD-GT8 60mer-immunized	10		<50	<50	<50	1,205	78	<50	<50	<50	<50	<50	<50
eOD-GT8 60mer-immunized	11		<50	<50	<50	523	74	<50	<50	<50	<50	<50	<50
eOD-GT8 60mer-immunized	12		<50	<50	<50	567	<50	<50	<50	<50	<50	<50	<50
BG505 SOSIP-immunized	13		178	141	2,522	1,895	1,004	563	<50	589	424	113	134
BG505 SOSIP-immunized	14		<50	<50	5,049	2,419	1,381	647	<50	670	306	<50	235
BG505 SOSIP-immunized	15		<50	<50	2,054	2,118	1,336	78	<50	228	<50	<50	<50
BG505 SOSIP-immunized	16		<50	<50	4,990	3,116	2,107	105	72	585	148	<50	56
BG505 SOSIP-immunized	17		<50	<50	1,525	4,741	1,771	51	60	63	<50	<50	54
BG505 SOSIP-immunized	18		<50	<50	1,637	1,850	1,396	1,548	86	68	<50	<50	52
BG505 SOSIP-immunized	19		<50	<50	1,879	1,715	907	454	50	91	<50	<50	<50

Figure 11: Neutralizing activity in TZM-bl assays of serum from individual naive, eOD-GT8 60-mer- or BG505 SOSIP-immunized mice (M) against a panel of HIV-1 viruses. Numbers indicate the reciprocal dilution of serum at the median inhibitory concentration (IC50): red, >1,000; orange, 100-1000; yellow, 50-100, and white, not neutralized at any dilution tested. Gray indicates background activities against the control MuLV virus.

eOD-GT8-binding IgG+ B cells cannot be detected in naive MuVH mice but increase to 15% and 30% after immunization with eOD-GT8 60mers or BG505 SOSIP, respectively[2]. Thus, both antigens were able to induce clonal expansion of antigen-specific memory B cells. To characterize the antibodies that develop in the MuVH mice, we isolated and cloned the antibodies from antigen-specific memory B cells. As expected, all of the heavy chains obtained carried the MuVH knock-in sequence. A total of 138 and 269 light

chains were cloned from mice immunized with eOD-GT8 60mers and BG505 SOSIP, respectively (Figure 12). The antibodies obtained from eOD-GT8 60mer-immunized mice represent 15 independent clones ranging in size from 2-24 members, 4 of the clones appeared independently in both sequenced eOD-GT8 60mer-immunized mice. In addition there were 13 cells that carried unique sequences (Figure 12A). In contrast to the antibodies obtained from eOD-GT8 60mer-immunized GLVH mice, the light chains from MuVH immunized mice were highly biased to express 5 aa-residue CDRL3s (Figure 12B). Moreover, the fourth residue in the CDRL3 was highly selected for an E, which is an important residue in the 3BNC60 antibody and other VH1-2-class antibodies. It forms a contact with the backbone of the V5 loop of HIV-1 Env[1,79,98] (Figure 12).

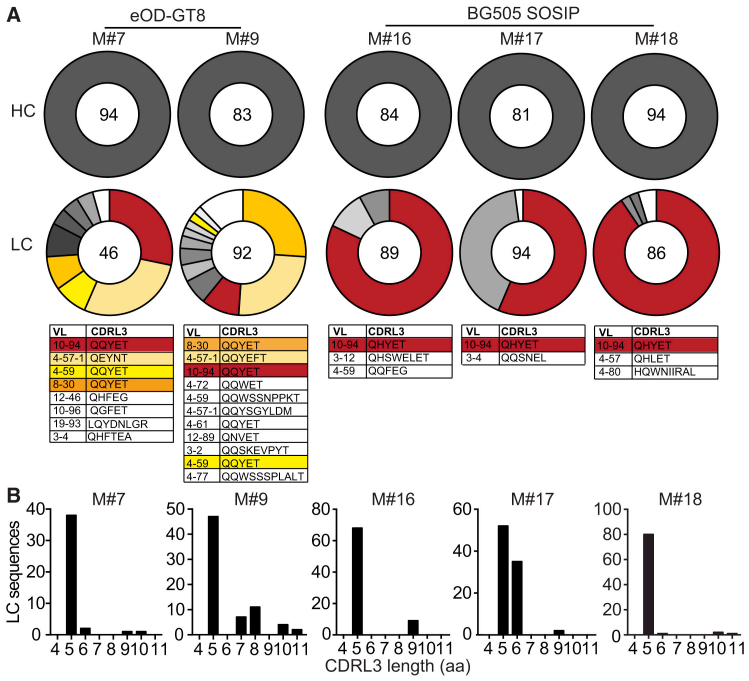

Figure 12A: Pie charts show heavy- (HC) and light-chain (LC) sequences cloned from two eOD-GT8 60-mer-immunized (M#7 and 9) and three BG505 SOSIP-immunized (M#16, 17, and 18) MuVH mice. VL gene usage and CDRL3 sequences are shown for each clone; colors correspond to colors in pie charts. The same color indicates clones shared by different mice. A clone is defined by identical V gene and similar CDRL3. B: CDRL3 aa lengths of the LCs in (A).

When assayed by ELISA, the majority of these antibodies were CD4bs specific to eOD-GT8, and a fraction was cross-reactive to YU2 gp140-F (Figure 13).

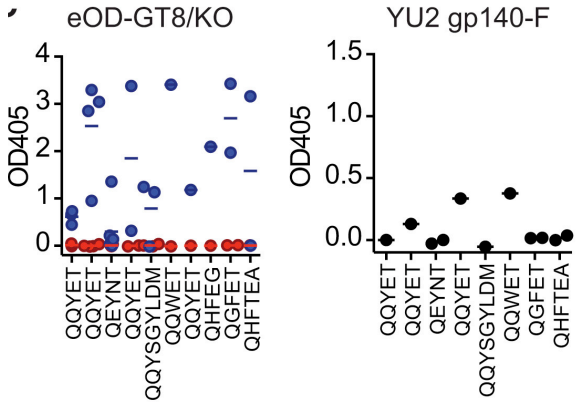

Figure 13: Graphs show ELISA results for individual monoclonal antibodies with the indicated CDRL3s cloned from eOD-GT8 60-mer-immunized MuVH mice against eOD-GT8 (blue) and eOD-GT8 CD4bs knock-out (KO, red) (at 0.55 µg/ml) or against YU2 gp140-F (at 5 µg/ml).

However, despite CD4bs specificity, only two viruses (T247-2 and 62357.14.D3.3489, which lack glycosylation at amino acid position 276) were neutralized by the monoclonal antibodies tested (Figure 14).

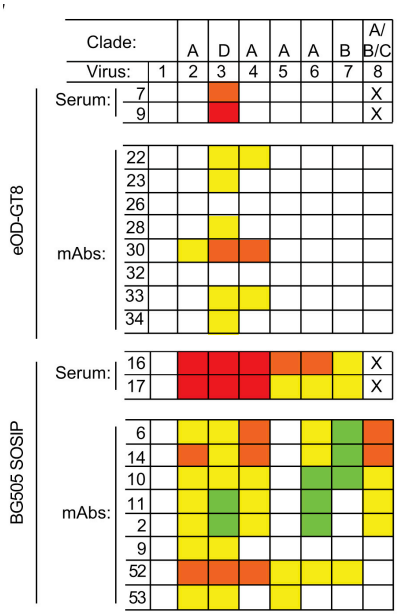

Figure 14: Neutralizing activity of a set of representative eOD-GT8 60-mer- or BG505 SOSIP-elicited monoclonal antibodies against 7 HIV-1 tier 2 viruses (1 = MuLV control, 2 = BG505/T 332N, 3 = T247-23, 4 = 62357.14.D3.3489, 5 = Q842.d12, 6 = 3365.V2.c30, 7 = YU2.DG, and 8 = 0815.v3.c3) compared to the serum of the mouse they were cloned from. Colors for monoclonal antibodies indicate concentration of monoclonal antibody at the median inhibitory concentration (IC50): orange, 0.1 to 1 µg/ml; yellow, 1 to 10 µg/ml; green, 10-25 or 50 µg/ml and white, not neutralized at any concentration tested. Lowest dilution tested for serum was 1:50, highest concentration tested for monoclonal antibodies were between 10 and 50 µg/ml. X indicates sample not tested.

Thus, eOD-GT8 60mer-immunization of MuVH mice is highly selective for a subset of mouse light chains with short CDRL3s that allow binding to the CD4bs of eOD-GT8, but this is not sufficient to produce broad neutralizing activity against tier 2 viruses.

Antibodies cloned from BG505 SOSIP-immunized MuVH mice were far more clonally restricted than those obtained after eOD-GT8 60mer immunization.

Light chains were cloned from 269 cells from 3 separate mice, and again, in all cases analyzed the heavy chain was from the knock-in. In contrast to eOD-GT8 60mer, BG505 SOSIP-immunization was dominated by only six highly expanded clones, one of which arose independently in all three mice (Figure 12). Similar to eOD-GT8 60mer-immunization, the B cell clones expanded by BG505 SOSIP-immunization were highly biased to express light chains with 5 aa-residue CDRL3s that carry the E at the fourth position of CDRL3 (Figure 12). When tested by ELISA, all but 4 of the 20 antibodies elicited by BG505 SOSIP were CD4bs specific on eOD-GT8 and a fraction of these were cross-reactive to YU2 gp140-F (Figure 15).

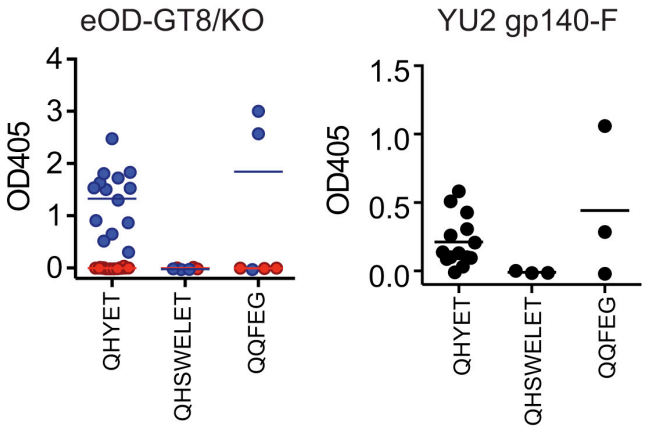

Figure 15: Graphs show ELISA results for individual monoclonal antibodies with the indicated CDRL3s cloned from BG505 SOSIP-immunized MuVH mice against eOD-GT8 (blue) and eOD-GT8 CD4bs knock-out (KO, red) (at 0.55 µg/ml) or against YU2 gp140-F (at 5 µg/ml).

Finally, some of these monoclonal antibodies showed neutralizing activity against several tier 2 viruses (Figure 14). We conclude that in contrast to eOD-GT8-, BG505 SOSIP-immunization elicits neutralizing antibodies against a diverse group of tier 2 viruses in MuVH mice.

2.4 SOMATIC MUTATIONS

Only the antibodies arising from BG505 SOSIP-immunization neutralized clade A and B tier 2 viruses (Figure 14). To gain further insight into this phenomenon we analyzed the monoclonal antibodies and somatic mutations that arose during the immunization.

The total number of light chain mutations arising as a result of immunization by the eOD-GT8 60mer or BG505 SOSIP was similar in both strains of mice, irrespective of whether the knock-in heavy chain was germline or mature (Figure 16A). In addition, both immunogens selected for B cells bearing the same VL germline gene (VL10-94*01) carrying similar number of somatic mutations and nearly identical CDRL3s in MuVH mice (Figure 12A, 16B). Thus, the nature of the immunogen did not influence the rate of somatic mutations in the light chains.

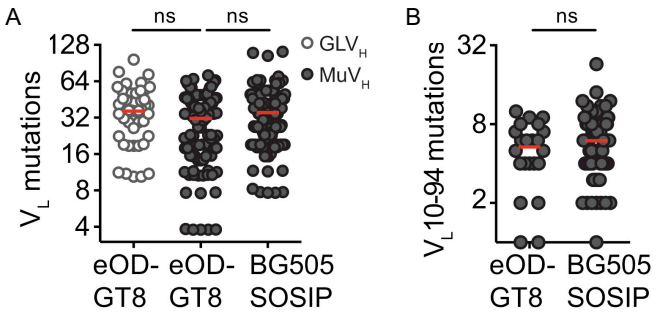

Figure 16A: Graph shows number of light-chain (LC) somatic hypermutations in individual sequences obtained after eOD-GT8 60-mer or BG505 SOSIP immunization in GLVH or MuVH mice. B: LC somatic hypermutations in VL10-94*01 in individual sequences obtained after eOD-GT8 60-mer or BG505 SOSIP immunization in MuVH mice. Y axes on graphs indicate nucleotide mutations/1,000 bp. Red lines in all graphs indicate the mean of the group.

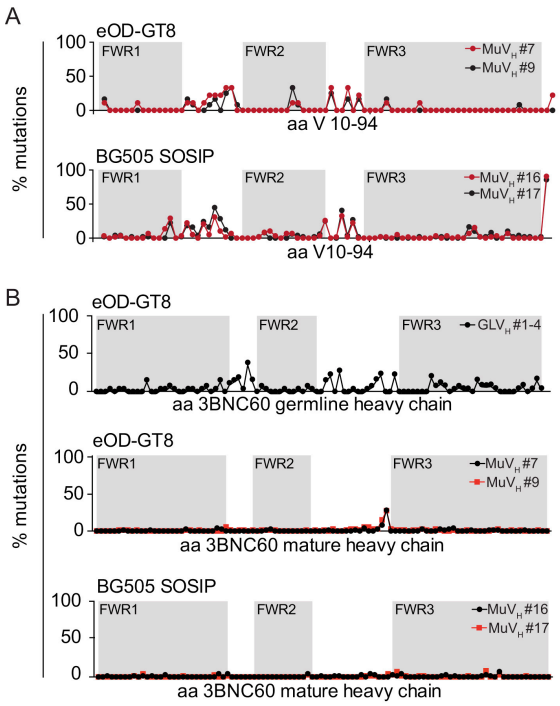

Figure 17A: Light chain somatic mutation analysis of VL10-94 sequences in eOD-GT8 60-mer- (top) and BG505 SOSIP- (bottom) immunized MuVH mice. Amino acid (aa) positions of the framework 1-3 (FWR1-3, gray background) and complementarity determining regions (white background) are indicated. B: Somatic mutation analysis of the germline (top) and mature (middle and bottom) sequences after immunization with eOD-GT8 60-mer (top and middle) or BG505 SOSIP (bottom).

For example, Q90H was found in the 2nd position of CDRL3 of nearly all members of the VL10-94 clone obtained independently from three MuVH mice immunized with BG505 SOSIP but rarely in the VL10-94 clone that arose after immunization with eOD-GT8 60mers (Figure 17). While others such as the E mutation found in the 4th residue of CDRL3 was selected by both immunogens. Thus immunization with BG505 SOSIP and eOD-GT8 60mers led to differential selection of somatically mutated light chains.

To determine whether light chain mutations might be responsible for increasing neutralizing activity after BG505 SOSIP immunization, we produced an antibody that carries the MuVH and the predicted germline light chain of VL10-94*01 (GL in Figure 18). When this antibody was compared to BG505 SOSIP-derived monoclonal antibodies (mAbs), the reverted antibody showed only modest activity. The reverted antibody was similar to the eOD-GT8 60mer-derived VL10-94*01 mAbs indicating that only BG505 SOSIP-immunization selects for light chain somatic mutations that increase neutralizing antibody activity in MuVH mice (Figure 18). Moreover, the Q90H found in the CDRL3 of nearly all VL10-94-expressing clones derived from BG505 SOSIP-immunized MuVH mice was sufficient to increase neutralizing activity (Figure 18). Additional mutations that further enhanced or interfered with neutralizing activity appeared randomly (Figure 18). Finally, there was no evidence for selection of specific mutations in the heavy chain in MuVH B cells as seen by the absence of significant clonal expansion of any particular mutation (Figure 17B).

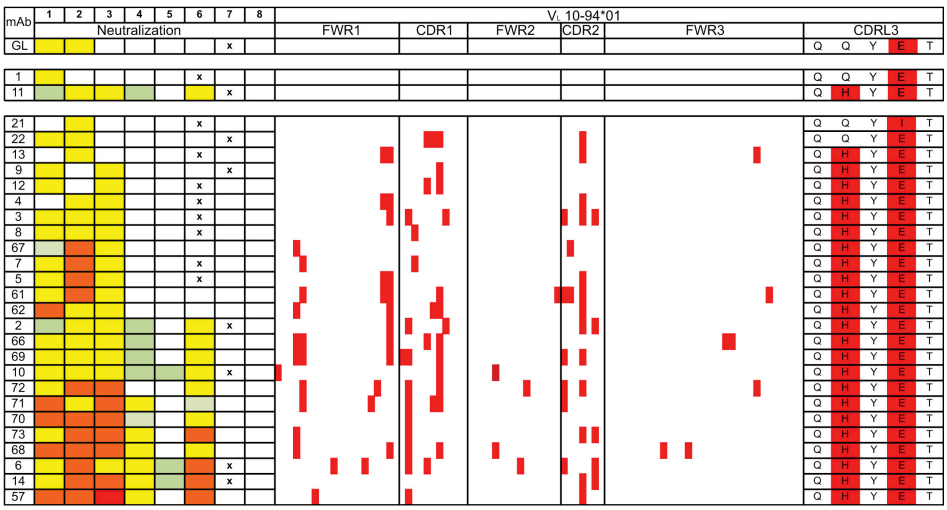

Figure 18: VL10-94*01 germline (GL) and 17 monoclonal antibodies from immunized MuVH mice sorted by neutralization strength. Neutralization data for each antibody tested against virus 1 = T247-23, 2 = 62357.14.D3.3489, 3 = BG505/T332N, 4 = 3365.v2.c30, 5 = YU2.DG, 6 = 0815.v3.c3, 7 = HxBC2.DG, and 8 = MuLV. Colors for monoclonal antibodies indicate concentration of monoclonal antibody at the median inhibitory concentration (IC50): red, <0.1 µg/ml; orange, 0.1 to 1 µg/ml; yellow, 1 to 10 µg/ml; green, 10-25 or 50 µg/ml and white, not neutralized at any concentration tested. X indicates sample not tested. Position of aa mutations in the LCs compared to germline is highlighted in red.

In contrast to the light chains, mutations in the knock-in VDJ-HC sequence were significantly higher in GLVH than in MuVH B cells (Figure 19A) even when comparing Peyer's Patch germinal center B cells in unimmunized mice that are not responding to injected antigens (Figure 19B). However, the mutation rate in the germline intron downstream of JH4, which is contiguous to the VDJ-HC, was similar in the two mouse strains (Figure 19C). We conclude that the somatic mutation machinery is equally active in the two knock-in B cell types, but the highly mutated MuVH is less susceptible to further mutations than its unmutated GLVH counterpart.

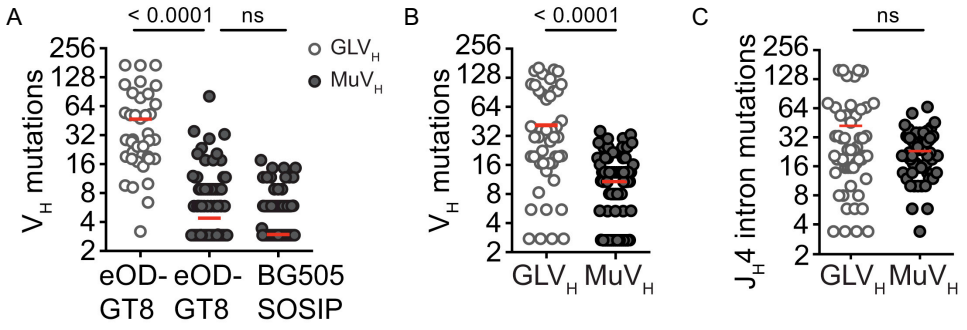

Figure 19A: Somatic hypermutations in individual heavy-chain (HC) sequences obtained after eOD-GT8 60-mer or BG505 SOSIP immunization in GLVH or MuVH mice. Data in (A) are pooled from 9 mice. B: Somatic hypermutations in individual germinal center B cell HC sequences obtained from naive GLVH or MuVH mice. C: Somatic hypermutations in individual germinal center B cell JH4 intron sequences obtained from naive GLVH or MuVH mice. Data in B and C are pooled from two independent experiments with two to three mice each. 60-80 clones were sequenced for GLVH or MuVH germinal center B cells HC and JH4. Y axes on graphs indicate nucleotide mutations/1,000 bp. Read lines in all graphs indicate the mean of the group.

CHAPTER 3: AN EASIER ROADMAP

We succeeded in inducing broad tier 2 neutralizing antibodies in Ig KI mice, but our study established that the protein based vaccination regimen will need at least two proteins and many obstacles still have to be overcome to achieve this result in humans. That is why we sought to identify a broad neutralizing antibody with properties that might be easier to induce by vaccination. In this chapter I will describe IOMA, a new broadly neutralizing antibody. IOMA constitutes a new class of CD4-mimetic bNAb derived from the VH1-2 germline, with a normal-length CDRL3 and fewer somatic hypermutations than the other VH1-2-CD4bs-class bNAbs. We defined IOMA's complete epitope by using crystal structures of a fully and natively glycosylated Env trimer. Besides IOMA being an intriguing vaccine design template, we analysed the native glycan shield on Env providing what is, to our knowledge, the first full description of the heterogeneous untrimmed high-mannose and complex-type N-glycans on Env.

3.1 ISOLATION OF IOMA

I isolated IOMA by single memory B-cell sorting[55] from an HIV-1/Hepatitis C co-infected ART-treated patient (R1) from Germany. R1 started ART four months after initial diagnosis. ART treatment was paused twice for 2.5 years at 17 months and 7 years after treatment initiation, and for 3 months ~11 years after initiation. 17 years after diagnosis a leukapheresis was performed from which IOMA was isolated.

IOMA was part of the second largest clone using gp140-foldon or BG505-SOSIP as baits (Figure 20).

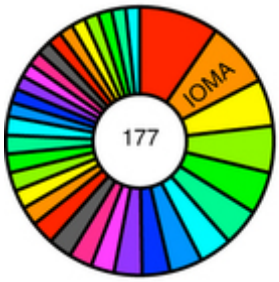

Figure 20: Pie chart showing IgG HC clones of single-cell-sorted HIV-1-antigen-specific memory B cells from patient R1. The number in the center is the number of sequences considered: each colored slice represents one clone, and the slice size is proportional to the number of clonal sequences.

IOMA accounts for most of the neutralizing activity in this patient's serum, as demonstrated by a comparison of neutralization activities of serum IgG and purified IOMA (Figure 21).

Virus	Clade (tier)	R1 IC_{50} (µg/mL)	IOMA IC_{50} (µg/mL)
BaL.26	B (1B)	13.73	0.05
Q23.17	A (1B)	67.76	0.83
R2184.c04	CRF01_AE (2)	81.27	>50
YU2.DG	B (2)	139.76	0.13
ZM249M.PL1	C (2)	194.40	16.58
MuLV		>500	>78

Figure 21: Comparison of neutralizing activity of subject-R1 serum IgG and IOMA, an antibody cloned from the second-largest clone of the IgG+ sorted memory B cells.

Unlike other CD4bs bNAbs, IOMA has relatively few somatic hypermutations (22 heavy chain and 15 light chain amino acid changes from the germline, as compared with 41 and 25 changes for VRC01), yet IOMA neutralized ~50% of tested strains with a mean half-maximal inhibitory concentration (IC50) of 2.3 µg/mL and a breadth and potency superior to those of CD4bs bNAbs with

similar somatic hypermutation rates (for example, b12) but inferior to those of CD4bs bNAbs with more somatic hypermutations[1,45] (Figure 22).

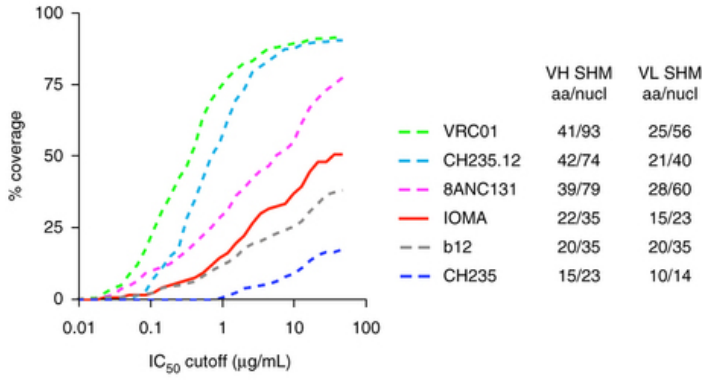

Figure 22: Neutralization coverage curves for selected CD4bs bNAbs. The number of somatic hypermutations (including indels) at the level of amino acids (aa) and nucleotides (nucl) are indicated for VH and VL gene segments. CH235 is an earlier member of the lineage that produced CH235.12[45].

As mentioned before, IOMA is an interesting target for structural studies because it combines features of VH1-2-class bNAbs with a second related but distinct set of CD4-mimetic CD4bs bNAbs derived from the VH1-46 germline gene segment[99]. Like VH1-46, but unlike VH1-2 bNAbs, IOMA includes a normal-length (eight residue) CDRL3.

3.2 COMPARISON OF IOMA WITH OTHER CD4-MIMETIC bNAbs

Although the Env binding orientation of IOMA differed somewhat from the orientations of both VH1-2-class and VH1-46-class bNAbs, the IOMA-BG505 SOSIP interaction shared CD4-mimetic features of both bNAb classes, including the R71HC-D368gp120 interaction and CDRH2 mimicking the C″ strand of CD4[97,99] (Figure 23).

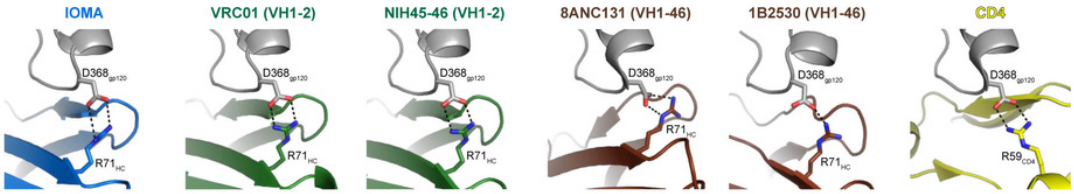

Figure 23: Interactions of Env residue D368gp120 with residue R71HC of IOMA and indicated bNAbs. Interactions of Env with CD4 residue R59CD4.

VH1-2-class bNAbs are distinguished from VH1-46-like bNAbs by their five-residue CDRL3s, W50HC (VH1-2 germline encoded), and CDRH3-encoded residue W100BHC[3]. IOMA contains a W50HC, but, in contrast to VH1-2-class bNAbs, this residue does not contact gp120 (Figure 23 and 24). IOMA also includes a counterpart of the signature CDRH3 W100BHC residue in VH1-2-class bNAbs. In VH1-2-class bNAbs, this tryptophan (Kabat numbering 100B; usually located four residues before the CDRH3 C terminus) is the most conserved antigen-facing residue within the CDRH3, and its side chain indole nitrogen hydrogen-bonds with a side chain oxygen of N279gp120 (Figure 25B).

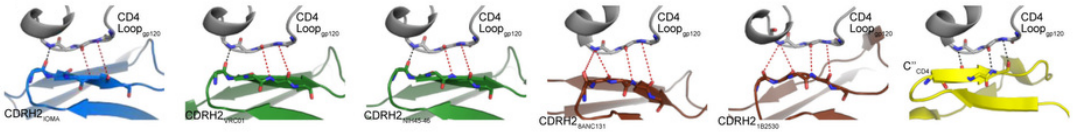

Figure 24: Interactions of the CD4-binding loop in gp120 with CDRH2 of IOMA and indicated bNAbs and with the C" strand of CD4. Black dashed lines indicate potential hydrogen bonds; red dashed lines indicate potential hydrogen bonds with non-ideal geometry.

The IOMA HC includes a tryptophan five residues from the C-terminal end of CDRH3 (Kabat numbering 100F). IOMA's W100FHC preserved the interactions observed for VH1-2-class W100BHC with N279gp120/N280gp120 (Figure 25B).

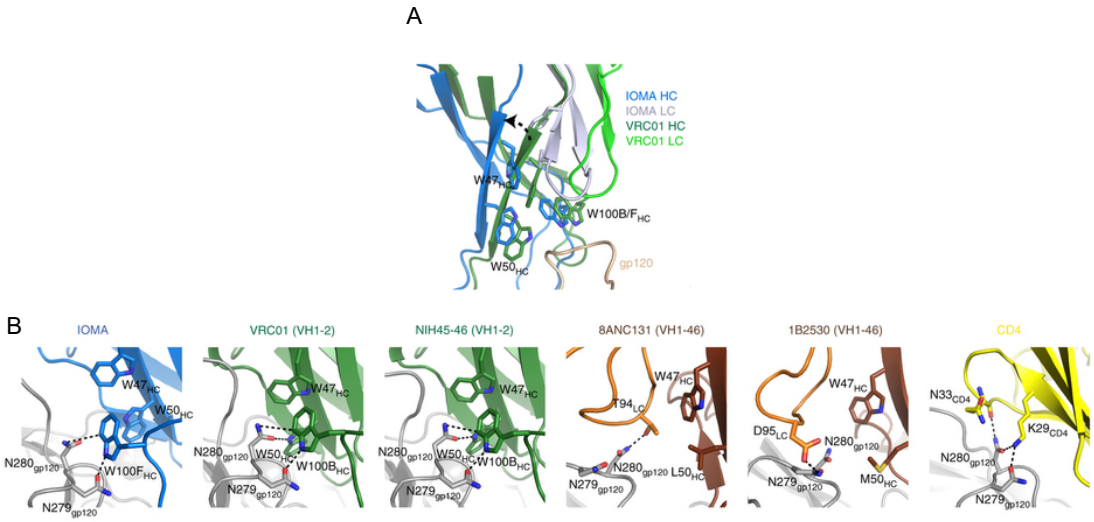

Figure 25A: Shift in IOMA's FWRH2 β-strand. To accommodate IOMA's normal-length CDRL3, there is a shift relative to VRC01 in IOMA's FWRH2 β-strand; thus, IOMA residue W50HC does not interact with gp120. B: Interactions of W100BHC (W100FHC in IOMA) with N279gp120/N280gp120 in indicated bNAbs and CD4.

VH1-46-like bNAbs use their normal-length CDRL3s in place of a W100BHC residue to interact with N279gp120/N280gp120 (Figure 25B). IOMA is unique in having both an N279gp120/N280gp120-W100FHC interaction and a normal-length CDRL3, a combination made possible because its CDRL3 is displaced from gp120 loop D and toward the V5 loop (Figure 26). We further addressed the question of how IOMA recognizes Env with a normal-length CDRL3 together with signature VH1-2-class residues by comparing Env interactions with IOMA, VH1-2-class, and VH1-46-class bNAbs. In VH1-46-class bNAbs, the longer CDRL3 interacts with N279gp120/D279gp120 (Figure 25B), and the C-terminal portion of CDRH3 is farther from loop D.

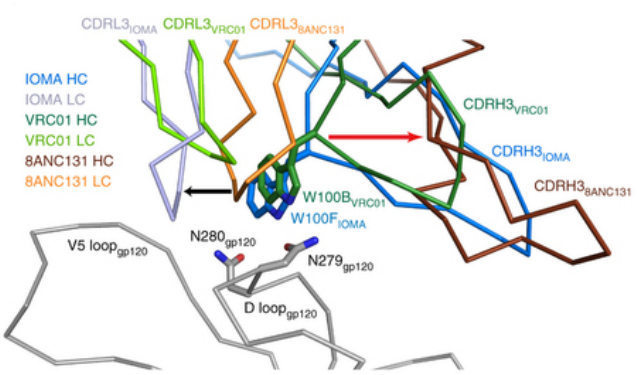

Figure 26: CDRL3 comparisons in CD4-mimetic antibody–Env complexes (aligned on the gp120s from the IOMA–10-1074–BG505 SOSIP(shown in gray) and the VRC01–gp120 (PDB 3NGB) and 8ANC131–gp120 (PDB 4RWY) structures). CDRL3s are light blue (IOMA), bright green (VRC01), and orange (8ANC131). The black arrow shows displacement of the eight-residue IOMA CDRL3 relative to the five-residue VRC01 CDRL3 away from W100FHC-IOMA and toward the gp120 V5 loop. The red arrow shows displacement of the CDRH3 in VH1-46-derived 8ANC131-like bNAbs (brown) relative to VRC01 class (dark green) and IOMA (dark blue) bNAbs.

In VH1-2-class bNAbs, E96LC (within a five-residue CDRL3) hydrogen-bonds with N280gp120 (Figure 27) and makes a backbone contact to G459gp120 (Figure 28).

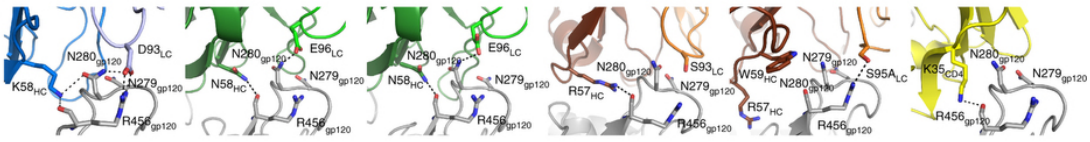

Figure 27: Interactions of CDRL3s with N279gp120/N280gp120. Blue = IOMA, green = VH1-2, brown = VH1-46 and yellow = CD4.

IOMA's eight-residue CDRL3 also includes a negatively charged residue, D93HC, that interacts with R456gp120 and N280gp120 (Figure 24 and 28).

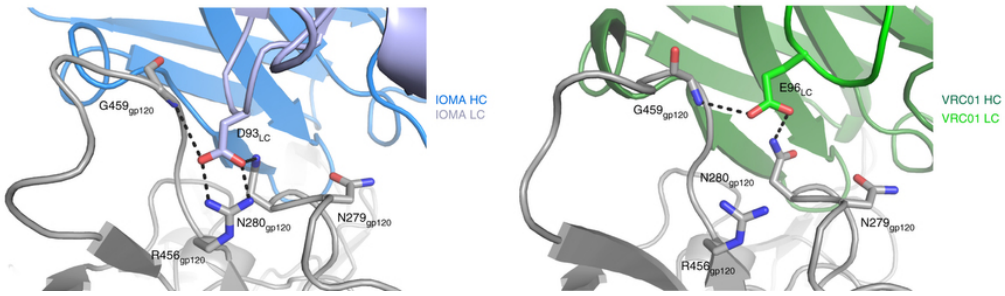

Figure 28: Comparison of structurally analogous acidic residues within the CDRL3s of IOMA (D93LC) and VRC01 (E96LC). Left, interface between gp120 (gray) and IOMA (HC, dark blue; LC, light blue), demonstrating interactions between IOMA D93LC and gp120 residues R456gp120, G459gp120, and N280gp120. Right, interface between gp120 (gray) and VRC01 (HC, dark green; LC, light green) demonstrating interactions between VRC01 E96LC and residues G459gp120 and N280gp120.

However, IOMA's longer CDRL3 is accommodated by a shift in BG505's gp120 V5 loop, relative to its position in gp120s complexed with VH1-2-class bNAbs, that allows IOMA's CDRL3 to penetrate the groove between the V5 and D loops (Figure 27 and 29).

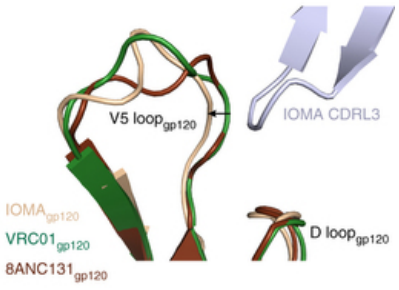

Figure 29: V5-loop shift. To accommodate IOMA's normal-length CDRL3, there is a shift in BG505's V5 loop in the IOMA-10-1074-BG505 SOSIP structure compared with V5 loops in complex structures of gp120s bound to VRC01 and 8ANC131.

IOMA's D93LC-R456gp120 interaction is not found in VH1-2-class bNAbs, wherein N58HC interacts with the backbone of R456gp120. In IOMA, the VH1-2 germline residue N58HC is mutated to K58HC, which interacts with the backbone of N280gp120, a similar interaction to that in 8ANC131 (Figure 27). The hydrophobic gp120 pocket, which normally accommodates F43CD4[111] and has been targeted by engineered substitutions of G54HC in VH1-2-class bNAbs[96], is filled by R54HC (Figure 30), as seen in a gp120-complex structure with 1B2530, a VH1-46-derived bNAb[99].

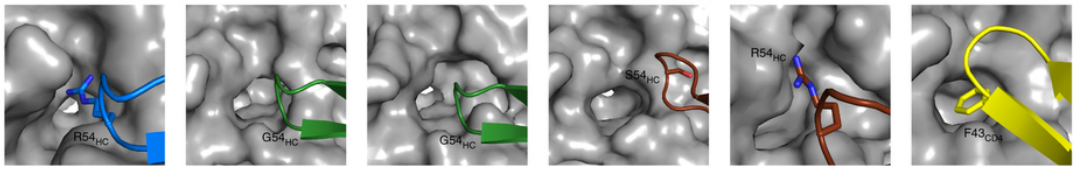

Figure 30: Interactions with the F43CD4 pocket on gp120. Blue = IOMA, green = VH1-2, brown = VH1-46 and yellow = CD4.

3.3 NATIVELY GLYCOSYLATED ENV TRIMER

HIV-1 Env is among the most heavily glycosylated proteins ever characterized[112]. It includes glycans, constituting up to 50% of its mass, attached to 30 ± 3 potential N-linked glycosylation sites (PNGSs) per gp120–gp41 protomer. Viral glycans are generally nonimmunogenic because they are assembled by the host-cell machinery; thus, carbohydrates decorating the surface of Env constitute a 'glycan shield' that reduces access to underlying protein epitopes[111]. Structural studies of bNAbs bound to Env trimers have revealed mechanisms by which bNAbs targeting various epitopes penetrate the glycan shield to either accommodate or include N-glycans in their epitopes[92-94,113-116]. The structure of the HIV-1 Env glycan shield itself, however, remains incompletely characterized. Previous trimer crystal structures have included Env produced in cells that attached only high-mannose-type N-glycans[93,94,113-115], which, with two exceptions[93,94], were

enzymatically trimmed to reduce glycans to single N-acetylglucosamines (GlcNAcs) at accessible PNGSs.

Because of steric constraints that limit the activities of endoplasmic reticulum and Golgi carbohydrate-processing enzymes, the HIV-1 Env glycoprotein includes regions of underprocessed N-glycans in oligomannose forms (Man5–9GlcNAc2), particularly in the intrinsic mannose patch on gp120, which forms portions of the epitopes for many characterized HIV-1 bNAbs[117]. Although oligomannose glycans dominate parts of HIV-1 Env, such as the N332gp120 glycan–associated region on gp120, processed complex-type N-glycans predominate at N-linked glycosylation sites on gp41 and gp41-proximal regions of gp120[118] and are thought to protect the host receptor (CD4)-binding site (CD4bs) and the V3 loop of gp120[119]. The IOMA and 10-1074 complexed crystals Harry Gristick developed in Pamela Bjoerkman's laboratory were obtained from natively glycosylated BG505 SOSIP produced in human cells that attached both complex-type and high-mannose N-glycans. He solved independent structures of the IOMA–10-1074–BG505 SOSIP complex by using BG505 SOSIP protein prepared from different size-exclusion chromatography (SEC) fractions (Figure 31) at resolutions of 3.5 Å and 3.9 Å.

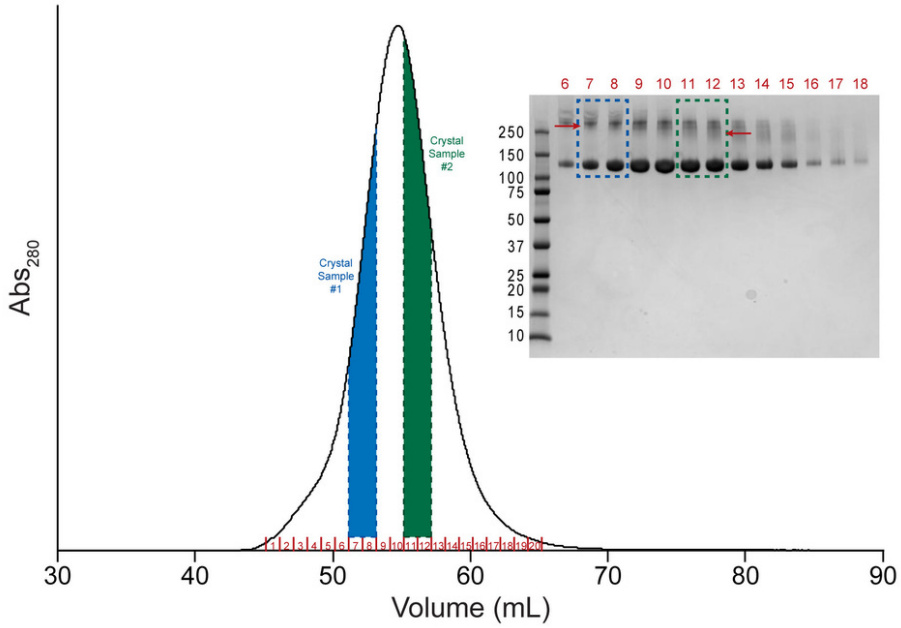

Figure 31: Size exclusion chromatography (SEC) profile showing migration of the BG505 SOSIP used for incubation with IOMA and 10-1074 Fabs to generate samples for crystallization. Inset shows SDS-PAGE analysis under non-reducing conditions of SEC fractions. SEC fractions 7-8 (blue) (larger apparent molecular mass; likely more glycosylated) were used for the 3.9Å IOMA–10-1074–BG505 SOSIP structure and fractions 11-12 (smaller apparent molecular mass; likely less glycosylated) were used for the 3.5Å IOMA–10-1074–BG505 SOSIP structure.

The IOMA–10-1074–BG505 SOSIP structures revealed an Env trimer bound to three 10-1074 and three IOMA Fabs (Figure 32).

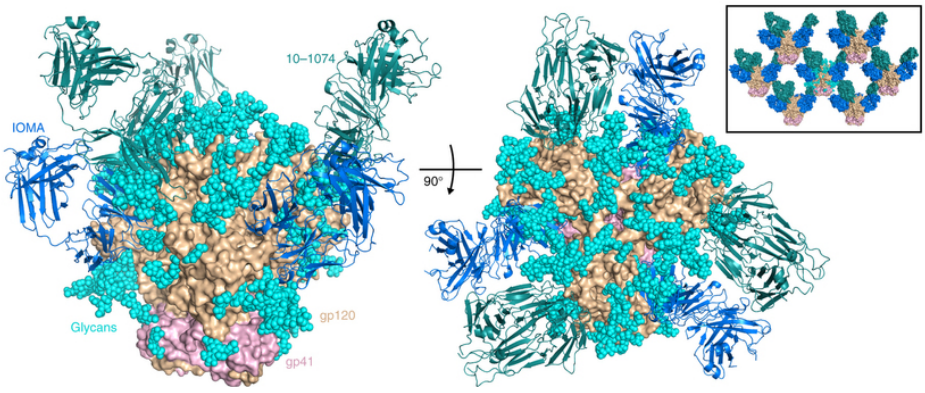

Figure 32: Side and top views of the IOMA–10-1074–BG505 SOSIP structure. Fabs are shown as ribbons, BG505 SOSIP is shown in surface representation, and glycans are shown as cyan spheres. Inset, packing in IOMA–10-1074–BG505 SOSIP crystals, demonstrating that the lattice is formed through interactions between neighboring Fabs.

19 N-glycans (one GlcNAc up to complex-type tetra-antennary) were visible per gp120–gp41 protomer, forming arrays of glycans extending ~30 Å from the trimer surface (Figure 33A-C). We observed N-glycan differences in the Env portions of the 3.5-Å- and 3.9-Å-resolution structures (Figure 33A).

Figure 33A: Top, BG505 SOSIP portion of IOMA–10-1074–BG505 SOSIP structure with complex-type (magenta) and high-mannose-type (cyan) N-glycans shown as spheres on the 3.9-Å- and 3.5-Å-resolution structures. Middle and bottom, BG505 SOSIP with 2Fo − Fc electron density contoured at 0.8σ for ordered glycans from model-phased (middle) or composite annealed omit (bottom) maps for the 3.9-Å- and 3.5-Å-resolution structures. B: Comparison of glycosylation in Env structures (side view). PGT121INT refers to the 3H + 3L intermediate that arose during maturation of PGT121[115]. Ordered N-glycans are shown as magenta (complex type) and blue (high mannose) spheres. C: First and third panels, surface area accessible to a 1.4-Å probe (red) shown on natively glycosylated BG505 SOSIP (3.9-Å-resolution structure; complex-type and high-mannose glycans are cyan spheres). Regions of gp120 and gp41 that are not surface accessible are shown in wheat and pink, respectively. Binding sites for IOMA (blue) and 10-1074 (green) are highlighted. Second and fourth panels, glycans displayed on the BG505 SOSIP surface, with sequence conservation among 116 HIV-1 strains color-coded from white (low sequence identity) to purple (high sequence identity). Arrow points to N241gp120 (yellow sphere in first panel), a PNGS in 97% of HIV-1 strains but not in BG505 SOSIP. The dotted ovals in the first two panels indicate an N241gp120-adjacent region of low sequence conservation that also lacks glycan density (same region shown on two adjacent protomers in each panel), which may represent an antibody-vulnerable glycan hole that would be targeted by strain-specific antibodies.

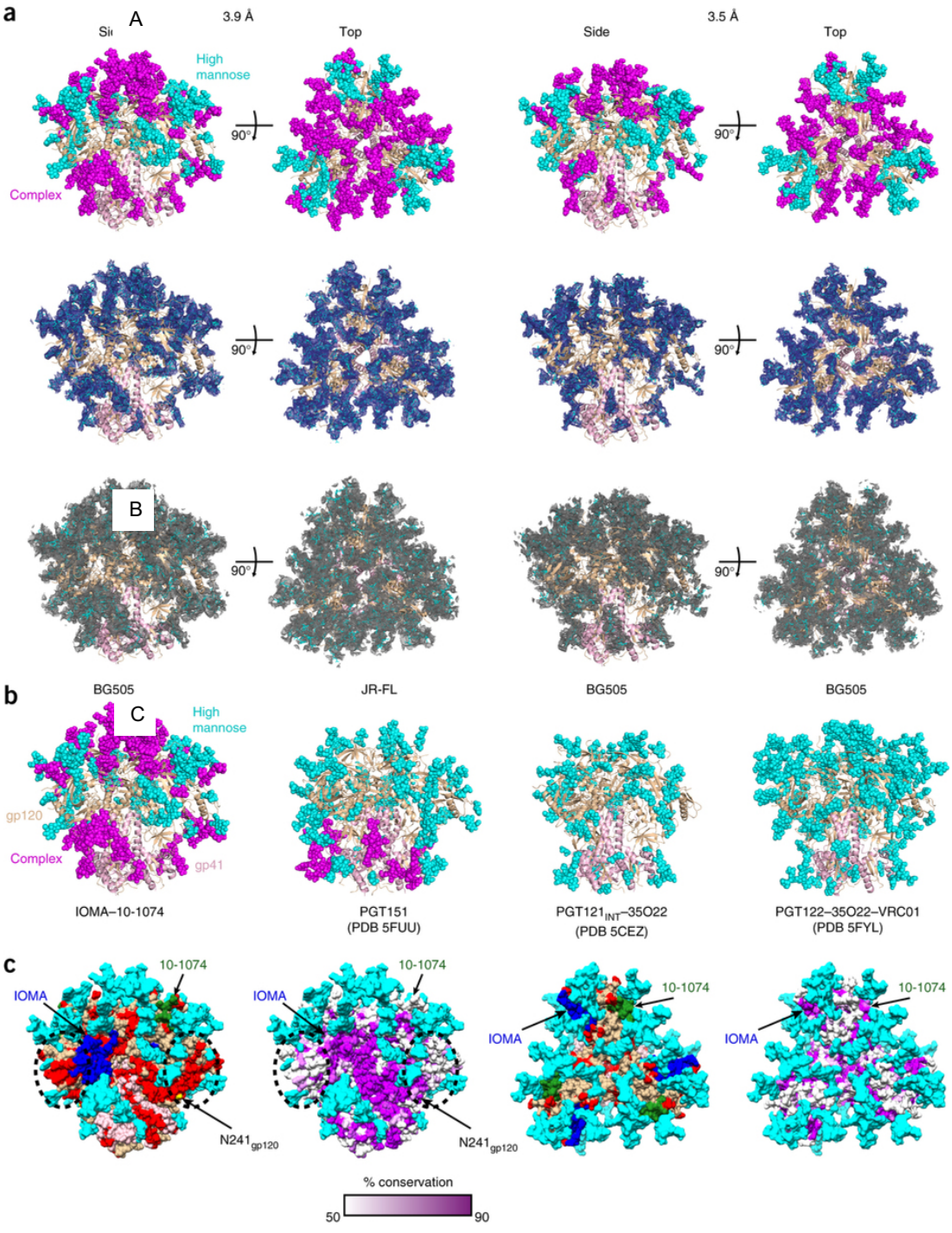
a
A
3.9 Å
Top
High mannose
90°
Complex
3.5 Å
Side
Top
B
b
BG505
C
High mannose
gp120
Complex
gp41
JR-FL
BG505
BG505
IOMA–10-1074
PGT151 (PDB 5FUU)
PGT121INT–35O22 (PDB 5CEZ)
PGT122–35O22–VRC01 (PDB 5FYL)
c
10-1074
IOMA
N241gp120
% conservation
50
90

We interpreted glycans in the 3.9-Å and 3.5-Å IOMA–10-1074–BG505 SOSIP structures, although glycan heterogeneity complicated modeling, we were often able to assign glycans at individual PNGSs as complex type or high mannose. The 3.9-Å structure sometimes showed more density for individual BG505 SOSIP N-glycans than the 3.5-Å structure, a result consistent with the apparently greater degree of glycosylation suggested by the SEC and SDS–PAGE characteristics of the BG505 SOSIP protein in crystals used for the lower-resolution structure. We assigned glycans as complex type if there was density for a core fucose and/or on the basis of mass spectroscopy assignments[118,120]. A core fucose was sometimes visible in one structure but not the other. We therefore interpreted glycans at some individual PNGSs as having different compositions in the two structures; such heterogeneity is consistent with the multiple glycoforms at single PNGSs identified in preparations of BG505 SOSIP protein[118].

Although there are caveats regarding the modeling and the N-glycan coordinates[121], the crystal structures revealed a relatively high-resolution view of a native glycan-shield structure that could be used for assessments of the roles of complex-type N-glycans in antibody recognition and HIV-1 Env function.

By comparison with the 4.2-Å cryo-EM structure of a natively/fully glycosylated Env[116], we observed a more extensively glycosylated trimer. Particularly the V3 loop, the CD4bs, the apex and gp120-gp41-interface regions of the BG505 SOSIP trimer showed clusters of complex-type N-glycans not observed in fully (but not natively) glycosylated Env crystal structures[94] (Figure 33B).

3.4 IOMA INTERACTIONS WITH NATIVELY GLYCOSYLATED ENV TRIMER

The accessibility to the conserved CD4bs on gp120 is restricted by surrounding glycans that have, to date, been visualized involving Env proteins including only high-mannose N-glycans[94-99]. The IOMA Fab is framed on both sides by Env N197gp120 and N276gp120 glycans, interpreted as complex-type biantennary and tetra-antennary, respectively, in the 3.9-Å structure, with minor interactions with a high-mannose glycan at N363gp120. IOMA accommodates the N276gp120 glycan with a short α-helix in CDRL1 instead of the extended loop in other CD4-mimetic bNAbs (Figure 34A-B).

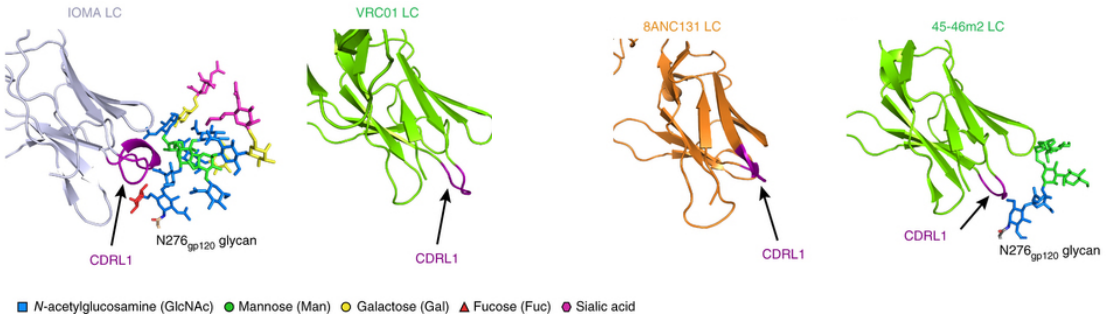

Figure 34A: LC of IOMA showing α-helical CDRL1 and N276gp120 glycan from the IOMA–10-1074–BG505 SOSIP structure. B: LC of VRC01 from a VRC01–gp120 structure (PDB 3NGB). The N276gp120 glycan was disordered in this structure. C: LC of 8ANC131 from an 8ANC131–gp120 structure (PDB 4RWY). The N276gp120 glycan was disordered in this structure. D: LC from 45-46m2 (an engineered VRC01-class bNAb13) from a 45-46m2–gp120 structure (PDB 4JKP). The N276gp120 glycan was partially ordered in this structure. Glycans are shown as sticks; color-coded as shown in key.

The need for CDRL1 to accommodate the glycan attached to N276gp120 is a barrier to the development of VH1-2-class bNAbs[97,99] that is typically overcome by CDRL1 deletions or by somatic hypermutations introducing

multiple glycine residues[98]. The VL2-23-derived CDRL1 of IOMA has no indels and is two or three residues longer than the CDRL1 of the common VH1-2-class LCs KV1-33 and KV3-20, and IOMA's CDRL1 acquired only one additional glycine residue during somatic hypermutation (G29LC). The short α-helix in IOMA's CDRL1 is a CDRL1 conformation not observed in available structures of VH1-2-class or VH1-46-class bNAbs (Figure 34). However, this helical conformation (designated L1-14-02 in refs.[122,123]) is common in the CDRL1s of antibodies derived from human germline VL2-23 and the closely related VL2-14 and VL2-8 germlines. For example, gp41-targeting bNAbs 3BC176 and 3BC315, which share germline VH and VL genes with IOMA, have CDRL1 loops in the same helical conformation as in IOMA (PDB 5AWN and 5CCK)[92]. VL2-14-derived bNAbs PG9, PG16, and 35O22 (PDB 3U4E, 4DQO, and 4TVP)[114,124,125] also include α-helical CDRL1s. Although VH1-2-class bNAb VRC-PG20 derives from VL2-14, its CDRL1 has a six-residue deletion and does not have a helical conformation[98].

In contrast with observed interactions in structures of VH1-2-class bNAb–Env complexes[95-99], IOMA interacts extensively with the Env N276gp120 and N197gp120 glycans. To compare how IOMA and other VH1-2-derived bNAbs accommodate these glycans, we evaluated the neutralization potencies of IOMA and VH1-2-class bNAbs against HIV-1YU2 pseudoviruses with N197gp120 or N276gp120 glycan deletions (Figure 35).

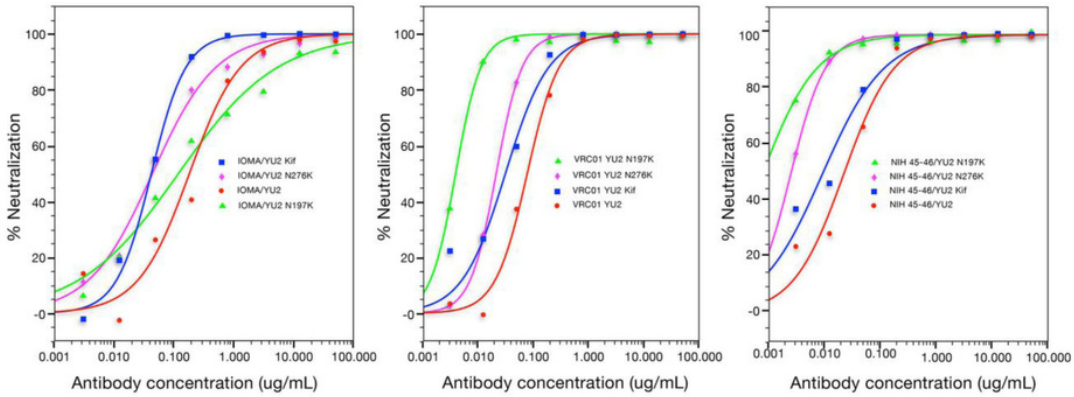

IC_{50} values (µg/mL)

Strain	IOMA	VRC01	NIH45-46
YU2	0.180	0.076	0.022
YU2 N276K	0.044	0.021	0.002
YU2 N197K	0.119	0.004	0.001
YU2 KIF	0.042	0.031	0.009

Figure 35: Comparison of glycosylation deletions on neutralization by IOMA and VH1-2-class bNAbs (VRC01 and NIH45-46). In vitro neutralization assays were conducted with HIV-1YU2 pseudoviruses that included all glycans (listed as YU2), had introduced mutations to remove the N276gp120 glycan (YU2 N276K), the N197gp120 glycan (YU2 N197K), or included all glycans in a high mannose form (YU2 Kif). Removal of glycans or conversion to high-mannose-only glycans had no effect (PNGS N197gp120) or increased IOMA's neutralization potency by ~4-fold (PNGS N276gp120 and high-mannose-only glycans). For VH1-2-class bNAbs, the same changes produced ~20-fold increased potency (PNGS N197gp120), ~4-11–fold increased potency (PNGS N276gp120), or ~2-fold increased potency (high-mannose-only glycans).

The results suggested that glycosylation at N197gp120 (98% conserved) is accommodated better by IOMA than by the VH1-2-class bNAbs VRC01 or NIH45-46, with both IOMA and the VH1-2-class bNAbs showing a slight preference for removal of the N276gp120 glycan (95% conserved). IOMA's similar ability to that of VRC01 for accommodating the N276gp120 glycan, one of the primary roadblocks in the development of VH1-2-class bNAbs[45,98],

required relatively small changes from its germline CDRL1 sequence. This aspect may favor the development of IOMA-like bNAbs and relate to IOMA's distinct Env-binding orientation and α-helical CDRL1 (Figure 36).

HC V gene	Antibody	LC V gene	Deleted residues	Extra glycines
VH1-2	VRC01	KV3-20*01	3	0
	NIH45-46	KV3-20*01	3	0
	VRC-PG04	KV3-20*01	3	0
	VRC-CH31	KV1-33*01	0	2
	12A12	KV1-33*01	0	3
	3BNC117	KV1-33*01	4	0
	VRC-PG20	LV2-14*01	6	0
	VRC18	KV3-20*01	0	1
	VRC23	KV3-15*01	0	2
	VRC27	KV1-5*01	0	2
	IOMA	LV2-23*02	0	1
	DRVIA7*	KV1-5*03	0	0
VH1-46	8ANC131	KV3-20*01	2	0
	8ANC134	KV3-20*01	2	0
	1B2530	LV1-47*01	0	2
	1NC9	LV1-47*01	0	1
	CH235	KV3-15*01	0	0
	CH235.12	KV3-15*01	0	0

Figure 36: Changes in CDRL1 versus germline for CD4-mimetic bNAbs. The mechanism by which each CDRL1 accommodates the N276gp120 glycan is highlighted in yellow. The reduced breadth and potency of DRVIA7 compared with other VRC01-class bNAbs appears to be due to its LC32.

CHAPTER 4: DISCUSSION

4.1 Immunization studies in the 3BNC60 knock in mouse model

To elicit a 3BNC60 antibody through vaccination, the immune system needs to mobilize B cells that express an IGHV1-2 heavy chain and a light chain with the 5-aa CDRL3. Light chains with 5-aa CDRL3 are rare in mice and humans, making the frequency of 3BNC60 precursors limited. In addition, 3BNC60 bears a high level of somatic hypermutations and although not all mutations are neutralization relevant, there is currently no way of directing mutations to a specific location, which means more mutations need to be inserted than the required neutralization relevant mutations. We evaluated the vaccination for 3BNC60 antibodies in our heavy chain 3BNC60 KI mice. The B cells in these mice have a reduced repertoire diversity because the heavy chain is fixed to express the 3BNC60 variable domain, but the light chains are recombining randomly. Importantly, the resulting naïve B cell repertoire does not contain more HIV-1 immunogen binding naïve B cells than wildtype mice. Immunization of mice bearing the predicted germline antibodies in their B cells could not be activated by native appearing HIV antigens but only responded to antigens specifically designed to bind to 3BNC60-like precursor antibodies. This result is consistent with the observation that the germline version of 3BNC60 and related antibodies fail to bind to nearly all tested recombinant HIV-1 Env antigens and supports the idea that specifically designed antigens are required to elicit B cells bearing these antibodies[100,103,104]. Through immunization with such a designed germline-targeting antigen (eOD-GT8 60-mer) we specifically seek to expand and further diversify rare clones of B cells that can serve as precursors of 3BNC60. Although rare in the pre-immune repertoire, GLVH B cells expressing antibodies with short CDRL3s were slightly enriched after immunization with the eOD-GT8 60-mer, providing proof of concept for

selection of germline precursors of this class of antibodies by germline targeting antigens.

In the mice bearing the MuVH KI heavy variable domain, both the engineered eOD GT8 and the native-like BG505 SOSIP trimer elicited antigen-specific B cell responses. Both types of antigens selected rare MuVH B cells expressing light chains with short CDRL3s and both induced similar levels of somatic hypermutation. Nevertheless, only immunization with BG505 SOSIP produced a significant neutralizing response. The response to the immunogens differed in two important ways. First, the repertoire of light chains that was selected to undergo clonal expansion by the native trimer was far more restricted than for the eOD-GT8 60-mer. This restriction is likely to be related to the glycan at position 276 that enforces the relatively narrow geometry of the recessed CD4 binding pocket in the trimer[87,111,126]. Under physiologic conditions, this cavity accommodates the single terminal Ig-like domain in CD4. Significant alterations must be made for the bulkier paired heavy- and light-chain Ig domains in 3BNC60 and related antibodies to access the CD4bs[127]. Many of these alterations are already present in the heavy chain of MuVH B cells, facilitating extensive contacts with gp120[127]. Nevertheless, the steric restrictions imposed by the glycan at 276 in BG505 SOSIP limit the number of light chains that can be recruited into the immune response against the trimer. In contrast, eOD-GT8 was designed to be more open and is missing the glycan at position 276. eOD-GT8 recruits a more diverse light chain repertoire than BG505 SOSIP immunization but the sets are overlapping in mice bearing the MuVH. Still none of the cloned antibodies from the eOD-GT8 immunized mice had significant breadth against tier 2 viruses in TZM-bl assays. The second difference between the two immunogens was in their ability to select for light chain mutations that enhance breadth and potency. In particular, the Q90H mutation that is selected in the BG505 SOSIP immunized mice in the CDRL3 of the VL10-94 light chains may aid in rigidifying the light chain contacts to the CD4bs.

Structural modeling of the VL10-94 light chain indicates that the histidine side chain, unlike the glutamine side chain, can adopt a commonly observed, low-energy conformation that also makes stabilizing interactions within the light chain. The planar packing with Y91, the close proximity to the N276 glycan, a hydrogen bond with CDRL1, and a potential for interacting with a gp120-bridging water molecule may help preconfigure the antibody for engagement of the CD4bs. The modeling and neutralization data indicate that the mutation could cause structural changes that influence binding to gp120 and may be necessary for the activity of the BG505 SOSIP elicited antibodies.

As mentioned above, achieving the right combination of aa substitutions for neutralization by random mutagenesis is a low probability event. Finding that the mature, fully mutated 3BNC60 VH suffers fewer mutations after immunization than the predicted germline 3BNC60 despite equal rates of somatic mutation in the light chains and in the JH4 intron suggests that the sequence of the VH is an important determinant of its susceptibility to hypermutation. Consistent with this idea, the fully mutated 3BNC60 VH has many fewer AID target sites than the predicted germline VH[128-130]. RGYW/WRCY are preferred targets for somatic hypermutation: 9 out of 12 RGYW and 7 out of 8 WRCY motifs found in GLVH sequence are missing in MuVH.

4.2 Immunization for VRC01-like antibodies

The VRC01 antibody, like 3BNC60, utilizes the IGHV1-2*02 heavy chain and has a short 5-aa CDRL3. The germline triggering immunogen we used, eOD-GT8, was also evaluated in a VRC01 KI mouse model[131]. In this model, the predicted germline VRC01 heavy chain was integrated into the mouse JH locus and as in the 3BNC60 model, the mouse LCs recombine randomly. CD4bs specific B cells after immunization with eOD-GT8 mainly had antibodies bearing a short, 5-aa CDRL3 mouse light chain. Similar to our

findings, these antibodies bound specifically to the CD4bs, but exhibited no neutralization activity. These results confirm that eOD-GT8 is an effective priming antigen. This group then evaluated a bridging immunogen between the eOD-GT8 and the native BG505 SOSIP. That immunogen, BG505coreGT3, contains fewer mutations than eOD-GT8 making its CD4bs more native-like and it binds mature VRC01-class antibodies with >1000-fold higher affinity than the germline reverted counterparts. Thus, boost immunization with BG505coreGT3 would promote the maturation of VRC01-like precursor antibodies. Using eOD-GT8, this intermediate immunogen and native Env trimers sequentially, the KI mice elicited CD4bs-specific antibodies that were composed of the VRC01 heavy chain and mouse LCs with 5-aa CDR L3. These antibodies acquired mutations corresponding to those found in VRC01-class broadly neutralizing antibodies. The elicited antibodies were able to neutralize tier 2 HIV-1 isolates with the N276 mutation and weakly neutralize the native form of this viral isolate that has the intact N276 glycosylation site. Other viral isolates with intact N276 glycosylation site remained refractory to neutralization by these and other cloned antibodies. Thus, these boosting regimens matured VRC01-like antibodies to an intermediate stage, validating the strategy of sequential immunization as an effective approach to mature VRC01-like antibodies.

Further critical questions have been addressed using the eOD-GT8 germline triggering immunogen: Do the targeted bnAb precursors exist in humans? What is the frequency and variation of germline-targeting immunogen–specific bnAb precursors? Can the germline-targeting immunogen bind the targeted human bnAb precursors in competition with other B cells in the divers human B cell repertoire? The results from epitope-specific B cell sorting from peripheral blood from healthy, HIV-seronegative donors, indicate that VRC01-class precursor B cells are relatively common in humans: At least 2’700 to 31’000 eOD-GT8–reactive VRC01-class naïve B cells are likely present in nearly all vaccine recipients. The data also suggest that eOD-GT8 has promise to produce VRC01-class memory even given competition from

non-VRC01-class B cells, as eOD-GT8 exhibited a high degree of CD4bs immunofocusing and VRC01-class precursors had an affinity advantage (factor of ≥3) over non-VRC01-class CD4bs epitope-binding precursors[138].

4.3 Immunization for PGT121-like antibodies

The PGT121 lineage targets the V3 and V1 regions near the apex of the Env trimer[57,132]. Induction of PGT121-class antibodies faces some of the same obstacle as those for CD4bs bNAbs: low precursor frequency and high SHM. In addition, PGT121 employs a 26-residue HCDR3 to penetrate through a glycan layer to interact with the underlying protein surface; such long HCDR3s are rare in the human or mouse antibody repertoire, like the short CDRL3 in CD4bs bNAbs. SHM frequencies for PGT121-class bnAbs, although lower than those of broadly neutralizing CD4bs antibodies, are still above average, and their light chains contain indels. Similar to the CD4bs bNAbs, the predicted germline reverted PGT121 antibody exhibits no binding affinity toward wildtype Env proteins[133,134]. The BG505 Env protein was engineered into a germline PGT121 binder, and proteins, closer to the wildtype Env, with fewer mutations and lower binding affinities for the germline PGT121, served as intermediate immunogens. The PGT121 immunogens were tested in two mouse models that express either the predicted germline PGT121 antibody, or a chimeric antibody composed of a mature PGT121 heavy chain and germline PGT121 light chain. Repeated immunization of these KI mice with native trimeric Env proteins failed to elicit any detectable antibody response. This was expected, as the germline and chimeric antibodies of PGT121 do not interact with native trimeric Env. In contrast, a single immunization with the germline-binding immunogen 10MUT was sufficient to elicit readily detectable autologous antigen-binding antibodies in the serum. Two intermediate protein immunizations followed this prime and after the third immunization, binding activity for native Env trimers was detectable in serum, leading to the logical step of using native BG505

trimer as the fourth boost. Finally, to broaden the immune response, a cocktail of native-like BG505 Env trimers with diverse variable loop sequences (VLC) was used. The neutralization breadth of the elicited antibodies was assessed on a panel of 54 tier 2 viruses and 2 tier 1B viruses. Antibodies from the full germline and chimeric PGT121 mice were able to neutralize 12 and 23 viruses in the test panel, respectively. Thus, this scheme of immunization could induce substantial breadth even starting with a full predicted germline antibody[133].

4.4 Immunization of Kymab mice

Although the heavy chain KI mouse models contain a diverse repertoire of antibodies, the frequency of B cells expressing the knocked in heavy chain is much higher than that in human antibody repertoire[135]. To evaluate a priming immunogen in a fully polyclonal environment, immunogens were tested in Kymab mice, in which the complete human IgH, Igκ, and Igλ variable region repertoire was incorporated into the corresponding mouse loci[136]. Remarkably, in spite of the paucity of VRC01-like class B cells in Kymab mice, immunization with eOD-GT8 60mer elicited CD4bs-specific antibodies, about 1% of which were composed of IGHV1-2 HC and various LCs with 5-aa CDRL3s. VRC01-like antibodies were detected in 29% of immunized Kymab mice. The mice were immunized only once and no neutralization activity was seen. And as expected, SOSIP Envs failed to elicit CD4bs- like bNAbs in the Kymab model[137].

In summary, immunization studies, done in various mouse models, have thus far provided several important insights. First, engineered immunogens, with high-affinity to the predicted germline of a bNAb can expand bNAb precursors, even in a polyclonal environment like in the Kymab mice. Second, sequential immunization with progressively more native-like Env immunogens is an effective way to mature bNAb precursor antibodies. It remains to be

seen, if the sequential immunization will lead to broad neutralization in the polyclonal environment or if it would induce irrelevant antibody responses, which may dominate over the development of bNAbs.

4.5 IOMA, an alternative CD4bs broad neutralizing antibody – implications for vaccine design

The isolation of IOMA and the IOMA-BG505 SOSIP structure revealed that VH1-2-derived CD4-mimetic bNAbs are not limited to five-residue CDRL3s and suggests an additional pathway for VH1-2-class bNAbs. A lot of focus is put on designing immunogens that bind to inferred VH1-2 germline precursors and select VH1-2 B-cells with short CDRL3s. As we have seen in the 3BNC60 KI mice, it will not be easy to select for these antibody chains due to their low frequency (~1% of LCs). The existence of CD4bs bNAbs with more favorable features has implications for immunization strategies. Many engineered CD4bs precursor antibody triggering immunogens selected B cells with longer CDRL3s, like IOMA. Studies using these immunogens should examine whether IOMA-like antibodies are elicited. Indeed, isolation of naive B cells binding to the VH1-2-class germline-targeting immunogen eOD-GT8 was found to enrich VH1-2-expressing cells from 4% to 50%, but 70% of eOD-GT8-binding/VH1-2-expressing cells do not express an antibody with a five-residue CDRL3; some or even most of these may represent B cells with IOMA-like antibody receptors[138]. Although the IOMA pathway may not lead to bNAbs with the breadth and potency of VH1-2-like bNAbs, it is possible that the IOMA pathway may more readily lead to an effective vaccine response, owing to higher frequencies of normal-length CDRL3s compared with the rare five-residue CDRL3s required for VH1-2-class bNAbs, and a lower need for somatic hypermutations.

4.6 Concluding remarks

Today, the most important diseases that used to kill or incapacitate millions are preventable by vaccination. Major efforts have been and are being put in vaccine development against HIV. The technological revolution we are experiencing currently (like single cell transcriptomics, CRISPR generated mice and structural biology), will help in the identification of vaccines against infectious agents that remain untargeted. We have used reverse and structural vaccinology, combined with synthetic biology to tackle the HIV vaccine problem.

CHAPTER 5: METHODS

Mice and Immunizations

Knockin mice were produced by gene targeting using the human VDJH sequences of the mature and germline 3BNC60 heavy chain[103]. The targeting vector was designed with homologous regions flanking the endogenous J segments, which results in the deletion of the J segments and thereby minimizes rearrangement of the wild-type locus. Mice were immunized once every 2 weeks with 10 μg of protein in Alum Imject (Thermo Scientific). Serum was collected 2 weeks after each immunization. All experiments were performed according to the protocols approved by the IACUC at Rockefeller University.

Protein Production

eOD-GT8 is an improved version of eOD-GT6[100,131]. The eOD-GT8 CD4bs knockout carries mutations to reintroduce the N276 glycan and also includes D368R and N279A. eOD-GT8 60-mer for immunization and monomers for ELISA detection were produced as previously described[100]. The 426c.TM4ΔV1-3 immunogen (with or without AviTag) is a derivative of the 426c.NLGS.TMΔV1-3[106] with the following additional modifications: D276N, S278R, and G471S (HXB2 numbering). The protein was produced as previously described[106]. Multimerized 426c.TM4ΔV1-3 was generated as follows: Avi-tagged and biotinylated 426c.TM4ΔV1-3 was mixed with streptavidin and biotinylated dextran (Life Technologies) at a 3:1 ratio of Env to biotin, with the assumption that the biotin had 77 biotin molecules/dextran. Streptavidin (New England Biolabs) was added to achieve a 3:1:1 Env to streptavidin to biotin ratio. To generate YU2 SOSIP.664, a gene encoding YU2 SOSIP.664 was constructed to include the “SOS” substitutions

(A501Cgp120 and T605Cgp41), the “IP” substitution (I559Pgp41), changing the gp120-gp41 cleavage site to 6R (REKR to RRRRRR) and introducing a stop codon after residue 664gp41 (HXB2 numbering) analogous to mutations introduced to generate BG505 SOSIP.664 as described[107]. YU2 SOSIP.664, BG505 SOSIP.664, and B41 SOSIP.664 (referred to as YU2 SOSIP, BG505 SOSIP, and B41 SOSIP) were produced and purified by the 2G12/SEC method as previously described[107,139,140]. YU2 gp140-F CD4bs knockout is a YU2 gp140-foldon (F) HIV-1 Env with A281T and D368K mutations, and proteins were produced as previously described[141].

ELISA

ELISA for eOD-GT8, eOD-GT8 CD4bs knock-out, YU2 gp140-F, YU2 gp140-F knock-out, YU2 SOSIP, and B41 SOSIP was performed by coating high binding 96-well plates (Corning Incorporated) with 200 ng/well of protein. After incubation overnight (ON) at 4°C, the plates were washed in wash buffer (PBS with 0.05% TWEEN 20 [Sigma]) and incubated in blocking buffer (PBS with 2% milk). Serum samples or monoclonal antibodies were added in dilutions. Plates were washed and secondary antibody, HRP conjugated anti-mouse or anti-human IgG (Jackson Immuno Research), was added. Plates were developed by the addition of HRP substrate (Life Technologies), and the absorbance was measured at 405 nm. ELISA specific for BG505 SOSIP was performed using the D7324-capture ELISA as described in[107].

TZM-bl Neutralization Assay

Serum samples and monoclonal antibodies were tested for neutralization against a panel of selected HIV-1 pseudoviruses using a TZM-bl neutralization assay as previously described[110].

IgGs for neutralization assays were expressed in HEK293-6E cells (National Research Council of Canada) by transient transfection of equal amounts of HC and LC vectors and purified by Protein G–Sepharose 4 Fast Flow Chromatography (GE Healthcare) from transfected cell supernatants collected after 7 d of culture. Sterile filtration and buffer exchange to PBS were performed before testing for neutralizing activity.

Pseudovirus neutralization was monitored by the reduction of HIV-1 Tat-induced luciferase reporter gene expression in the presence of a single round of pseudovirus infection in TZM-bl cells, as previously described50. Neutralization assays were conducted by the Collaboration for AIDS Vaccine Discovery (CAVD) core neutralization facility or in house. Data were fit in Prism (GraphPad) with nonlinear regression to derive IC50 values. The IC50 values were derived from independent replicates of manual and robotic assays conducted with eight potential inhibitor concentrations tested in duplicate or triplicate, and generally agreed within two- to four-fold. Average IC50 values reported in the figures and tables are geometric means calculated with the formula $(\prod ai)(1/N)$; i = 1, 2, ..., N. Geometric means are suitable statistics for data sets covering multiple orders of magnitude[142], as is the case for neutralization data across multiple viral strains. Fold improvements were calculated as the ratio of the geometric mean IC50 values for the reagents being compared.

B Cell Enrichment

B cells were enriched from single-cell suspensions of total splenocytes prior to flow cytometry staining by magnetic bead separation using anti-CD19 or anti-CD43 MicroBeads (Miltenyi Biotec). The separation was performed on MACS separation LS columns according to the manufacturer's instructions.

Flow Cytometry

Single-cell suspensions of total splenocytes, enriched B cells, or BM were stained with different combinations of the following antibodies: anti-CD4 APC-eFluor 780, anti-CD8 APC-eFluor 780, anti-Gr1 APC-eFluor 780, anti-F4/80 APC-eFluor 780, anti-B220 APC, anti-B220 APC-eFluor 780, anti-B220 FITC, anti-CD19 PeCy7, anti-CD38 Alexa Fluor 700, anti-CD93 APC, anti-IgM PerCP-eFluor 710, anti-CD21/CD35 eFluor 450 and anti-GL7 eFluor 660 (eBiosciences), anti-CD23 PE (BioLegend), anti-CD4 PE-CF594, anti-CD8 PE-CF594, anti-Ly-6G and Ly-6C PE-CF594, anti-IgG1 and CD95 BV421 (BD Biosciences). Live dead aqua stain was added to separate dead cells (Life Technologies), and eOD-GT8-specific cells were visualized by the addition of FITC-conjugated eOD-GT8 and PE-conjugated eOD-GT8 CD4bs knockout. BG505 SOSIP-[60] and 2cc-specific memory B cells were visualized by the addition of biotinylated protein with the addition of streptavidin-conjugated PE and APC, respectively (BD Biosicences)[102].

B Cell Sorting

Staining and single-cell sorting of naive and memory B cells was performed as follows: for naive mice, CD4-, CD8-, Gr-1-, F4/80-, B220+, and IgM+ B cells were sorted. For immunized mice, CD4-, CD8-, Gr-1-, F4/80-, B220+, CD38-, IgM-, IgG+, eOD-GT8 CD4bs knockout and eOD-GT8+ or CD4-, CD8-, Gr-1-, F4/80-, B220+, CD38-, IgM-, IgG+, BG505 SOSIP+, and 2cc+ memory B cells were single-cell sorted into 96-well plates using a FACSAria III sorter (Becton Dickinson). The cells were lysed with 4 µl lysis buffer containing RNASin (Promega) 40 U/µl (0,3 µl), DPBS (Dulbecco) 10× (0.2 µl), DTT (Invitrogen) 100 mM (0.4 µl), and nuclease-free water (3.1 µl). The sorted plates were stored at −80°C until further procecessing. Sequencing and cloning primers are listed in Table S6. Antibodies were cloned using a

modified sequence and ligation-independent cloning (SLIC) approach as described in[102]. Antibodies were produced in HEK293-6E cells as described in[102]. Bulk sorted GC B cells were amplified with the following primers: pF: GGGATGGTCATGTATCATCCTTTTTCTAGTAGC and p279: TCCTAGGAACCAACTTAAGAGT.

gp140YU2 and 2cc-core were used for sorting experiments with R1 and were produced as previously described[1]. Purified total B cells were stained with combinations of anti-human CD19 (FITC human CD19 (BD, 340864)), IgG (APC human IgG (BD, 550931)) antibodies and PE-labeled gp140YU2 or 2cc-core. Antigen-specific IgG+ memory B cells were single-cell-sorted on a BD Aria cytometer into 96-well PCR plates containing 4 µL/well of lysis buffer. Plates were immediately frozen on dry ice before storage at −80 °C. For each cell, cDNA was generated by two-step reverse transcription with random primers. The sequences of the VH and VL domains were amplified by nested PCR, with a combination of previously described primers[1,102,143]. Sequence analysis was performed to identify Ig gene usage, HC and LC CDR3s, and the number of VH-VL somatic hypermutations (IgBLAST, http://www.ncbi.nlm.nih.gov/igblast/ and IMGT, http://www.imgt.org/). For cloning by PCR, the primers contained 15–20 base pairs of 5′ and 3′ homology to restriction-digested expression vectors to allow for cloning by homologous recombination into DH5α[102].

Structural Modeling

To create a structural model of one of the antibodies elicited in the MuVH mouse by BG505 SOSIP, we integrated information from HIV bNAb structures and mouse light-chain structures. The antibody 3BNC117 has very high sequence similarity to 3BNC60 (ten mutations in heavy chain and three mutations in light chain[1]) and has a co-crystal structure available (PDB: 4JPV). We made an initial model of 3BNC60 by running 50 ROSETTA-

Fixbb[144] simulations to model the mutations from the 3BNC117 structure. The elicited antibodies contain a mutated mouse light chain from the VL10-94*01 germline gene; here, we focused on the Q90H mutation. To model the light chain, we used an unrelated crystal structure of a mouse VL10-94*01 antibody (PDB: 1EMT). We superimposed the mouse antibody to the 3BNC60 model and created a hybrid of 3BNC60-mature heavy chain and VL10-94*01 light chain to mimic what was elicited in MuVH. The 1EMT structure did not contain a five aa CDRL3, so we aligned the light chain from 3BNC117 and grafted the five amino CDRL3 onto our model. The final model was obtained by adding an interfacial water molecule (as found in the structurally similar VRC-CH31 light chain; PDB: 4LSP) and by running 100 ROSETTA-Relax simulations to allow for slight movements of the backbone.

Statistical Analysis

Statistical differences were analyzed by the Mann-Whitney test. GraphPad Prism software was used for analysis, and data were considered significant at $*p \leq 0.05$, $**p \leq 0.01$, and $***p \leq 0.001$.

Patient samples

Subject R1 is an HIV-1-infected individual who started antiretroviral therapy (ART) four months after initial diagnosis. ART treatment was paused twice for 2.5 years at 17 months and 7 years after treatment initiation, and for 3 months approximately 11 years after initiation. A serum sample was collected under informed written consent and in accordance with the University of Cologne Institutional Review Board (09–281). The serum sample was heat-inactivated for 1 h at 56 °C, and the IgG fraction was purified with Protein G–Sepharose 4 Fast Flow (GE Healthcare). Sterile filtration and buffer exchange to PBS was

performed before testing for neutralizing activity. IgG was screened for neutralizing activity against a panel of tier 1, tier 1B, and tier 2 viruses representing eight different clades or interclade recombinants. A leukapheresis sample (17 years after initial HIV-1 diagnosis) was obtained under informed consent and under approval of the Rockefeller University Institutional Review Board (MNU-0628). The sample was processed within 2 h of collection. Serum and plasma samples were stored, and PBMCs were isolated by density gradient centrifugation. The absolute number of peripheral blood mononuclear cells was determined with an automated cell counter (Vi-Cell XR; Beckman Coulter), and cells were cryopreserved in FBS/10% DMSO.

Protein production and purification for crystallography

Fabs from the IOMA and 10-1074 bNAbs (in which the 10-1074 Fab included a C263SLC substitution[145]) were expressed and purified as described in previous studies5. Briefly, Fabs were expressed by transient transfection in HEK293-6E cells (obtained from the National Research Council of Canada; tested for mycoplasma) with expression vectors containing genes encoding the LC and a C-terminally histidine-tagged Fab portion of the HC. Histidine-tagged Fabs were purified with Ni2+–NTA affinity chromatography (GE Healthcare) and SEC with a Superdex 200 16/60 column (GE Healthcare).

A gene encoding BG505 SOSIP.664, a soluble clade A gp140 trimer[107], was constructed to include 'SOS' substitutions (A501Cgp120 and T605Cgp41), the 'IP' substitution (I559Pgp41), the N-linked glycan sequence at residue 332gp120 (T332Ngp120), an enhanced gp120–gp41 cleavage site (REKR to RRRRRR), and a stop codon after residue 664gp41 (Env numbering according to HX nomenclature). Protein was expressed in HEK293-6E cells (National Research Council of Canada) by transient transfection of plasmids

encoding BG505 SOSIP and soluble furin at a ratio of 4:1, as previously described5, except that the cells were not treated with kifunensine. BG505 SOSIP protein was isolated from cell supernatants with a 2G12 immunoaffinity column made by covalently coupling 2G12 IgG monomer to an NHS-activated Sepharose column (GE Healthcare). After elution with 3 M MgCl2 and immediate buffer exchange into Tris-buffered saline, pH 8.0 (TBS), trimers were purified with Superdex 200 16/60 SEC (GE Healthcare). The trimer fractions were pooled and repurified with the same column. Twelve 1.0-mL fractions were collected, which were pooled in groups of two and then stored separately. Selected fractions were combined with IOMA and 10-1074 Fabs, thus resulting in two crystal structures: a 3.9-Å-resolution structure from BG505 fractions 7 and 8, and a 3.5-Å-resolution structure from BG505 fractions 11 and 12.

Crystallization

Samples for crystallization were produced by incubation of BG505 SOSIP with a 1:1:1 molar ratio of IOMA and 10-1074 Fabs for ~16 h at room temperature. The resulting complex was concentrated to 5–10 mg/ml with a 30-kDa concentrator (Amicon). Crystal trials were carried out with the sitting-drop vapor-diffusion method at room temperature by equilibration of equal volumes of the protein complex solution and reservoir solution with a TTP LabTech Mosquito robot and commercially purchased kits (Hampton Research). Crystals of IOMA–BG505–10-1074 complex (one BG505 protomer per asymmetric unit) were obtained by combining 0.2 µL of protein sample with 0.2 µL of 200 mM ammonium citrate tribasic, pH 7.0, 100 mM imidazole, pH 7.0, and 20% PEG MME 2000 at 20 °C. Crystals were cryoprotected in mother liquor supplemented with 20% glycerol and incubated for at least 10 min before being flash frozen in liquid nitrogen.

Crystallographic data collection, structure determination, and refinement

All structures were solved with data sets collected at 100 K and 1-Å resolution on Beamline 12-2 at the Stanford Synchrotron Radiation Lightsource (SSRL) with a Pilatus 6M pixel detector (Dectris). Data sets were indexed, integrated with MOSFLM53, and then merged with AIMLESS in the CCP4 software package54. A 3.9-Å-resolution structure of IOMA–10-1074–BG505 was solved with four data sets collected from crystals prepared with early fractions from the BG505 SEC purification, and a 3.5-Å-resolution structure was solved with 14 data sets collected from crystals prepared with later BG505 fractions. The 3.9-Å-resolution structure was solved by molecular replacement with a monomeric gp120–gp41 from BG505 SOSIP (PDB 4TVP), one copy of 10-1074 Fab (PDB 4FQ2), and one copy of a chimeric Fab (PDB 4TNN for the LC and PDB 4XVS for the HC) identified as a suitable model for IOMA by the FFAS server[146]. Coordinates were refined with PHENIX v1.10.1-2155 (ref.[147]) with group B factor and TLS restraints. The presence of ~10% twinning was corrected for by refining with the twin operator k,h,–l for space group R3:H. Manual rebuilding was performed with Coot56. The 3.5-Å-resolution structure was solved with a refined model from the 3.9-Å-resolution structure. In both models, >90~ of the residues were in the favored region of the Ramachandran plot, whereas <1~≃ were in the disallowed regions.

Glycans were interpreted in both structures with 2Fo − Fc maps calculated with model phases and with composite annealed omit maps calculated with phases in which the model was omitted to reduce model bias[147]. Glycans were refined with PDB CArbohydrate REsidue check (pdbcare) (http://www.glycosciences.de/tools/pdb-care/), CArbohydrate Ramachandran Plot (carp) (http://www.glycosciences.de/tools/carp/), and Privateer[148]. In general, the glycans identified crystallographically at individual PNGSs on BG505 SOSIP.664 were found within the mixture of glycans assigned at these positions with mass spectroscopy[118]. However, the N-linked glycan

attached to N156gp120 was modeled as complex type in our structures but has been identified as high mannose (primarily Man9GlcNAc2) in mass spectrometry analyses of BG505 SOSIP.664 (ref.[118]). When we modeled a high-mannose glycan at this site and carried out refinement as described above, we found a slight increase (0.1%) in Rfree and electron density in addition to that accounted for by the high-mannose residues, including density for a core fucose. We also modeled the N-linked glycan attached to N392gp120 as containing a core fucose, but it has been identified as a Man9GlcNAc2/Man8GlcNAc2 mixture in BG505 SOSIP.664 mass spectroscopy studies[118]. When the core fucose was removed from the N392gp120 glycan coordinates, a subsequent refinement showed a minor increase in Rfree, and electron density for the fucose was preserved.

Buried surface areas were determined with PDBePISA57 and a 1.4-Å probe. Superimposition calculations were performed, and molecular representations were generated with PyMOL (http://www.pymol.org/) or UCSF Chimera[149]. PDBeFold59 was used to perform pairwise Cα alignments. The following distance and geometry criteria were used for assigning putative hydrogen bonds: a distance of <3.5 Å and an A-D-H angle of >90°. The maximum distance allowed for a van der Waals interaction of 4.0 Å. Hydrogen-bond and van der Waals interaction assignments should be considered tentative, owing to the relatively low resolutions of the structures.

Antibody approach-angle comparisons

The angles of approach for selected CD4bs bNAbs were compared as follows: the structure of CD4 in complex with HxBc2 gp120 (PDB 1GC1) was used as a reference structure for comparisons of angles of approach of Fab recognition of gp120s. The center of mass of the CD4 D1 domain was placed at the origin, and its principal axes of inertia were aligned with the Cartesian

axes with AMORE from the CCP4 suite[150]. The remainder of the PDB 1GC1 complex was then aligned with the centered CD4 D1 domain. To compare with other complexes, each Fab–gp120 complex was aligned with the 1GC1 gp120 chain with LSQMAN60. The transformation matrix between the aligned Fab–gp120 VH domain and the CD4 D1 domain was then calculated by LSQMANN

Accession codes

Coordinates and structure factors for BG505 SOSIP.664 in complex with IOMA and 10-1074 Fabs have been deposited in the Protein Data Bank under accession codes PDB 5T3Z (3.5-Å resolution) and PDB 5T3X (3.9-Å resolution). IOMA HC and LC gene sequences have been deposited in GenBank under accession codes KX610770 and KX610771, respectively).

CHAPTER 6: REFERENCES

1. Scheid, J. F. *et al.* Sequence and structural convergence of broad and potent HIV antibodies that mimic CD4 binding. *Science* **333,** 1633–1637 (2011).
2. Dosenovic, P. *et al.* Immunization for HIV-1 Broadly Neutralizing Antibodies in Human Ig Knockin Mice. *Cell* **161,** 1505–1515 (2015).
3. West, A. P., Diskin, R., Nussenzweig, M. C. & Bjorkman, P. J. Structural basis for germ-line gene usage of a potent class of antibodies targeting the CD4-binding site of HIV-1 gp120. *Proc. Natl. Acad. Sci. U.S.A.* **109,** E2083–90 (2012).
4. Stover, J., Bollinger, L., Hecht, R., Williams, C. & Roca, E. The impact of an AIDS vaccine in developing countries: a new model and initial results. *Health Aff (Millwood)* **26,** 1147–1158 (2007).
5. Harmon, T. M. *et al.* Exploring the Potential Health Impact and Cost-Effectiveness of AIDS Vaccine within a Comprehensive HIV/AIDS Response in Low- and Middle-Income Countries. *PLoS ONE* **11,** e0146387–18 (2016).
6. Medlock, J. *et al.* Effectiveness of UNAIDS targets and HIV vaccination across 127 countries. *Proc Natl Acad Sci USA* 201620788–160 (2017). doi:10.1073/pnas.1620788114
7. Buchbinder, S. P. *et al.* Efficacy assessment of a cell-mediated immunity HIV-1 vaccine (the Step Study): a double-blind, randomised, placebo-controlled, test-of-concept trial. *Lancet* **372,** 1881–1893 (2008).
8. Gilbert, P. B. *et al.* Correlation between immunologic responses to a recombinant glycoprotein 120 vaccine and incidence of HIV-1 infection in a phase 3 HIV-1 preventive vaccine trial. *J. Infect. Dis.* **191,** 666–677 (2005).
9. Gray, G. E. *et al.* Safety and efficacy of the HVTN 503/Phambili Study of a clade-B-based HIV-1 vaccine in South Africa: a double-blind, randomised, placebo-controlled test-of-concept phase 2b study. *The Lancet Infectious Diseases* **11,** 507–515 (2011).
10. Hammer, S. M. *et al.* Efficacy Trial of a DNA/rAd5 HIV-1 Preventive Vaccine. *N. Engl. J. Med.* **369,** 2083–2092 (2013).
11. Pitisuttithum, P. *et al.* Randomized, double-blind, placebo-controlled efficacy trial of a bivalent recombinant glycoprotein 120 HIV-1 vaccine among injection drug users in Bangkok, Thailand. *J. Infect. Dis.* **194,** 1661–1671 (2006).
12. Rerks-Ngarm, S. *et al.* Vaccination with ALVAC and AIDSVAX to prevent HIV-1 infection in Thailand. *N. Engl. J. Med.* **361,** 2209–2220 (2009).
13. Borrow, P. & Moody, M. A. Immunologic characteristics of HIV-infected individuals who make broadly neutralizing antibodies. *Immunol Rev* **275,** 62–78 (2017).
14. Abbas, A. R. *et al.* Immune response in silico (IRIS): immune-specific genes identified from a compendium of microarray expression data.

Genes Immun **6,** 319–331 (2005).
15. Simon, A. K., Hollander, G. A. & McMichael, A. Evolution of the immune system in humans from infancy to old age. *Proc. R. Soc. B* **282,** 20143085–9 (2015).
16. Chun, T. W. *et al.* In vivo fate of HIV-1-infected T cells: quantitative analysis of the transition to stable latency. *Nat. Med.* **1,** 1284–1290 (1995).
17. Gulick, R. M. *et al.* Treatment with indinavir, zidovudine, and lamivudine in adults with human immunodeficiency virus infection and prior antiretroviral therapy. *N. Engl. J. Med.* **337,** 734–739 (1997).
18. Hammer, S. M. *et al.* A controlled trial of two nucleoside analogues plus indinavir in persons with human immunodeficiency virus infection and CD4 cell counts of 200 per cubic millimeter or less. AIDS Clinical Trials Group 320 Study Team. *N. Engl. J. Med.* **337,** 725–733 (1997).
19. Perelson, A. S. *et al.* Decay characteristics of HIV-1-infected compartments during combination therapy. *Nature* **387,** 188–191 (1997).
20. Chun, T. W. *et al.* Presence of an inducible HIV-1 latent reservoir during highly active antiretroviral therapy. *Proc. Natl. Acad. Sci. U.S.A.* **94,** 13193–13197 (1997).
21. Chun, T. W. *et al.* Early establishment of a pool of latently infected, resting CD4(+) T cells during primary HIV-1 infection. *Proc. Natl. Acad. Sci. U.S.A.* **95,** 8869–8873 (1998).
22. Tsai, C. C. *et al.* Prevention of SIV infection in macaques by (R)-9-(2-phosphonylmethoxypropyl)adenine. *Science* **270,** 1197–1199 (1995).
23. Tsai, C. C. *et al.* Effectiveness of postinoculation (R)-9-(2-phosphonylmethoxypropyl) adenine treatment for prevention of persistent simian immunodeficiency virus SIVmne infection depends critically on timing of initiation and duration of treatment. *Journal of Virology* **72,** 4265–4273 (1998).
24. Otten, R. A. *et al.* Efficacy of postexposure prophylaxis after intravaginal exposure of pig-tailed macaques to a human-derived retrovirus (human immunodeficiency virus type 2). *Journal of Virology* **74,** 9771–9775 (2000).
25. Whitney, J. B. *et al.* Rapid seeding of the viral reservoir prior to SIV viraemia in rhesus monkeys. *Nature* **512,** 74–77 (2014).
26. Descours, B. *et al.* CD32a is a marker of a CD4 T-cell HIV reservoir harbouring replication-competent proviruses. *Nature* **94,** 13193–8 (2017).
27. Cohen, M. S., Shaw, G. M., McMichael, A. J. & Haynes, B. F. Acute HIV-1 Infection. *N. Engl. J. Med.* **364,** 1943–1954 (2011).
28. Keele, B. F. *et al.* Identification and characterization of transmitted and early founder virus envelopes in primary HIV-1 infection. *Proc. Natl. Acad. Sci. U.S.A.* **105,** 7552–7557 (2008).
29. Salazar-Gonzalez, J. F. *et al.* Genetic identity, biological phenotype, and evolutionary pathways of transmitted/founder viruses in acute and

early HIV-1 infection. *J Exp Med* **206,** 1273–1289 (2009).
30. Keele, B. F. *et al.* Low-dose rectal inoculation of rhesus macaques by SIVsmE660 or SIVmac251 recapitulates human mucosal infection by HIV-1. *J Exp Med* **206,** 1117–1134 (2009).
31. Abrahams, M. R. *et al.* Quantitating the Multiplicity of Infection with Human Immunodeficiency Virus Type 1 Subtype C Reveals a Non-Poisson Distribution of Transmitted Variants. *Journal of Virology* **83,** 3556–3567 (2009).
32. Haaland, R. E. *et al.* Inflammatory Genital Infections Mitigate a Severe Genetic Bottleneck in Heterosexual Transmission of Subtype A and C HIV-1. *PLoS Pathog* **5,** e1000274–13 (2009).
33. Li, H. *et al.* High Multiplicity Infection by HIV-1 in Men Who Have Sex with Men. *PLoS Pathog* **6,** e1000890–17 (2010).
34. Ndhlovu, Z. M. *et al.* Magnitude and Kinetics of CD8+ T Cell Activation during Hyperacute HIV Infection Impact Viral Set Point. *Immunity* **43,** 591–604 (2015).
35. Goonetilleke, N. *et al.* The first T cell response to transmitted/founder virus contributes to the control of acute viremia in HIV-1 infection. *J Exp Med* **206,** 1253–1272 (2009).
36. Tomaras, G. D. & Plotkin, S. A. Complex immune correlates of protection in HIV-1 vaccine efficacy trials. *Immunol Rev* **275,** 245–261 (2017).
37. Liao, H.-X. *et al.* Initial antibodies binding to HIV-1 gp41 in acutely infected subjects are polyreactive and highly mutated. *J Exp Med* **208,** 2237–2249 (2011).
38. Tomaras, G. D. & Haynes, B. F. HIV-1-specific antibody responses during acute and chronic HIV-1 infection. *Current Opinion in HIV and AIDS* **4,** 373–379 (2009).
39. Gray, E. S. *et al.* The Neutralization Breadth of HIV-1 Develops Incrementally over Four Years and Is Associated with CD4+ T Cell Decline and High Viral Load during Acute Infection. *Journal of Virology* **85,** 4828–4840 (2011).
40. Doria-Rose, N. A. *et al.* Breadth of human immunodeficiency virus-specific neutralizing activity in sera: clustering analysis and association with clinical variables. *Journal of Virology* **84,** 1631–1636 (2010).
41. Landais, E. *et al.* Broadly Neutralizing Antibody Responses in a Large Longitudinal Sub-Saharan HIV Primary Infection Cohort. *PLoS Pathog* **12,** e1005369–22 (2016).
42. Sather, D. N. *et al.* Factors associated with the development of cross-reactive neutralizing antibodies during human immunodeficiency virus type 1 infection. *Journal of Virology* **83,** 757–769 (2009).
43. Medina-Ramirez, M. *et al.* Broadly Cross-Neutralizing Antibodies in HIV-1 Patients with Undetectable Viremia. *Journal of Virology* **85,** 5804–5813 (2011).
44. Sather, D. N. *et al.* Emergence of Broadly Neutralizing Antibodies and Viral Coevolution in Two Subjects during the Early Stages of Infection

with Human Immunodeficiency Virus Type 1. *Journal of Virology* **88,** 12968–12981 (2014).
45. Bonsignori, M. *et al.* Maturation Pathway from Germline to Broad HIV-1 Neutralizer of a CD4-Mimic Antibody. *Cell* **165,** 449–463 (2016).
46. Gao, F. *et al.* Cooperation of B Cell Lineages in Induction of HIV-1-Broadly Neutralizing Antibodies. *Cell* **158,** 481–491 (2014).
47. Liao, H.-X. *et al.* Co-evolution of a broadly neutralizing HIV-1 antibody and founder virus. *Nature* **496,** 469–476 (2013).
48. Moody, M. A. *et al.* Strain-Specific V3 and CD4 Binding Site Autologous HIV-1 Neutralizing Antibodies Select Neutralization-Resistant Viruses. *Cell Host and Microbe* **18,** 354–362 (2015).
49. Burton, D. R. *et al.* Efficient neutralization of primary isolates of HIV-1 by a recombinant human monoclonal antibody. *Science* **266,** 1024–1027 (1994).
50. Conley, A. J. *et al.* Neutralization of divergent human immunodeficiency virus type 1 variants and primary isolates by IAM-41-2F5, an anti-gp41 human monoclonal antibody. *Proc. Natl. Acad. Sci. U.S.A.* **91,** 3348–3352 (1994).
51. Stiegler, G. *et al.* A potent cross-clade neutralizing human monoclonal antibody against a novel epitope on gp41 of human immunodeficiency virus type 1. *AIDS Res. Hum. Retroviruses* **17,** 1757–1765 (2001).
52. Zwick, M. B. *et al.* Broadly Neutralizing Antibodies Targeted to the Membrane-Proximal External Region of Human Immunodeficiency Virus Type 1 Glycoprotein gp41. *Journal of Virology* **75,** 10892–10905 (2001).
53. Simek, M. D. *et al.* Human immunodeficiency virus type 1 elite neutralizers: individuals with broad and potent neutralizing activity identified by using a high-throughput neutralization assay together with an analytical selection algorithm. *Journal of Virology* **83,** 7337–7348 (2009).
54. Seaman, M. S. *et al.* Tiered Categorization of a Diverse Panel of HIV-1 Env Pseudoviruses for Assessment of Neutralizing Antibodies. *Journal of Virology* **84,** 1439–1452 (2010).
55. Scheid, J. F. *et al.* Broad diversity of neutralizing antibodies isolated from memory B cells in HIV-infected individuals. *Nature* **458,** 636–640 (2009).
56. Walker, L. M. *et al.* Broad and potent neutralizing antibodies from an African donor reveal a new HIV-1 vaccine target. *Science* **326,** 285–289 (2009).
57. Walker, L. M. *et al.* Broad neutralization coverage of HIV by multiple highly potent antibodies. *Nature* **477,** 466–470 (2011).
58. Huang, J. *et al.* Broad and potent neutralization of HIV-1 by a gp41-specific human antibody. *Nature* **491,** 406–412 (2012).
59. Falkowska, E. *et al.* Broadly Neutralizing HIV Antibodies Define a Glycan-Dependent Epitope on the Prefusion Conformation of gp41 on Cleaved Envelope Trimers. *Immunity* **40,** 657–668 (2014).

60. Sok, D. *et al.* Recombinant HIV envelope trimer selects for quaternary-dependent antibodies targeting the trimer apex. *Proc. Natl. Acad. Sci. U.S.A.* **111,** 17624–17629 (2014).
61. Wibmer, C. K., Moore, P. L. & Morris, L. HIV broadly neutralizing antibody targets. *Current Opinion in HIV and AIDS* **10,** 135–143 (2015).
62. Huang, J. *et al.* Identification of a CD4-Binding-Site Antibody to HIV that Evolved Near-Pan Neutralization Breadth. *Immunity* **45,** 1108–1121 (2016).
63. Berek, C., Berger, A. & Apel, M. Maturation of the immune response in germinal centers. *Cell* **67,** 1121–1129 (1991).
64. Jacob, J., Kelsoe, G., Rajewsky, K. & Weiss, U. Intraclonal generation of antibody mutants in germinal centres. *Nature* **354,** 389–392 (1991).
65. Schwickert, T. A. *et al.* In vivo imaging of germinal centres reveals a dynamic open structure. *Nature* **446,** 83–87 (2007).
66. Allen, C. D. C., Okada, T., Tang, H. L. & Cyster, J. G. Imaging of germinal center selection events during affinity maturation. *Science* **315,** 528–531 (2007).
67. Victora, G. D. *et al.* Germinal Center Dynamics Revealed by Multiphoton Microscopy with a Photoactivatable Fluorescent Reporter. *Cell* **143,** 592–605 (2010).
68. Mouquet, H. *et al.* Polyreactivity increases the apparent affinity of anti-HIV antibodies by heteroligation. *Nature* **467,** 591–595 (2010).
69. Nemazee, D. A. & Bürki, K. Clonal deletion of B lymphocytes in a transgenic mouse bearing anti-MHC class I antibody genes. *Nature* **337,** 562–566 (1989).
70. Goodnow, C. C. *et al.* Altered immunoglobulin expression and functional silencing of self-reactive B lymphocytes in transgenic mice. *Nature* **334,** 676–682 (1988).
71. Meffre, E. *et al.* Immunoglobulin heavy chain expression shapes the B cell receptor repertoire in human B cell development. *J. Clin. Invest.* **108,** 879–886 (2001).
72. Wardemann, H. *et al.* Predominant autoantibody production by early human B cell precursors. *Science* **301,** 1374–1377 (2003).
73. Gitlin, A. D. *et al.* Independent Roles of Switching and Hypermutation in the Development and Persistence of B Lymphocyte Memory. *Immunity* **44,** 769–781 (2016).
74. Doria-Rose, N. A. *et al.* Developmental pathway for potent V1V2-directed HIV-neutralizing antibodies. *Nature* **508,** 55–62 (2014).
75. Klein, F. *et al.* Antibodies in HIV-1 vaccine development and therapy. *Science* **341,** 1199–1204 (2013).
76. Freund, N. T. *et al.* Coexistence of potent HIV-1 broadly neutralizing antibodies and antibody-sensitive viruses in a viremic controller. *Sci Transl Med* **9,** eaal2144 (2017).
77. Klein, F. *et al.* Antibodies in HIV-1 vaccine development and therapy. *Science* **341,** 1199–1204 (2013).

78. Escolano, A., Dosenovic, P. & Nussenzweig, M. C. Progress toward active or passive HIV-1 vaccination. *J Exp Med* **214,** 3–16 (2017).
79. Wu, X. *et al.* Rational design of envelope identifies broadly neutralizing human monoclonal antibodies to HIV-1. *Science* **329,** 856–861 (2010).
80. Klein, F. *et al.* Broad neutralization by a combination of antibodies recognizing the CD4 binding site and a new conformational epitope on the HIV-1 envelope protein. *J Exp Med* **209,** 1469–1479 (2012).
81. Bonsignori, M. *et al.* Two Distinct Broadly Neutralizing Antibody Specificities of Different Clonal Lineages in a Single HIV-1-Infected Donor: Implications for Vaccine Design. *Journal of Virology* **86,** 4688–4692 (2012).
82. Andrabi, R. *et al.* Identification of Common Features in Prototype Broadly Neutralizing Antibodies to HIV Envelope V2 Apex to Facilitate Vaccine Design. *Immunity* **43,** 959–973 (2015).
83. Doores, K. J. & Burton, D. R. Variable Loop Glycan Dependency of the Broad and Potent HIV-1-Neutralizing Antibodies PG9 and PG16. *Journal of Virology* **84,** 10510–10521 (2010).
84. Pejchal, R. *et al.* A potent and broad neutralizing antibody recognizes and penetrates the HIV glycan shield. *Science* **334,** 1097–1103 (2011).
85. Kong, L. *et al.* Supersite of immune vulnerability on the glycosylated face of HIV-1 envelope glycoprotein gp120. *Nat. Struct. Mol. Biol.* **20,** 796–803 (2013).
86. McCoy, L. E. & Burton, D. R. Identification and specificity of broadly neutralizing antibodies against HIV. *Immunol Rev* **275,** 11–20 (2017).
87. Julien, J.-P. *et al.* Asymmetric recognition of the HIV-1 trimer by broadly neutralizing antibody PG9. *Proc. Natl. Acad. Sci. U.S.A.* **110,** 4351–4356 (2013).
88. Huang, J. *et al.* Broad and potent HIV-1 neutralization by a human antibody that binds the gp41-gp120 interface. *Nature* **515,** 138–142 (2014).
89. Huang, J. *et al.* Broad and potent HIV-1 neutralization by a human antibody that binds the gp41-gp120 interface. *Nature* **515,** 138–142 (2014).
90. van Gils, M. J. *et al.* An HIV-1 antibody from an elite neutralizer implicates the fusion peptide as a site of vulnerability. *Nature Microbiology* **2,** 1–10 (2016).
91. Kong, R. *et al.* Fusion peptide of HIV-1 as a site of vulnerability to neutralizing antibody. *Science* **352,** 828–833 (2016).
92. Lee, J. H. *et al.* Antibodies to a conformational epitope on gp41 neutralize HIV-1 by destabilizing the Env spike. *Nature Communications* **6,** 1–14 (2015).
93. Scharf, L. *et al.* Broadly Neutralizing Antibody 8ANC195 Recognizes Closed and Open States of HIV-1 Env. *Cell* **162,** 1379–1390 (2015).
94. Stewart-Jones, G. B. E. *et al.* Trimeric HIV-1-Env Structures Define Glycan Shields from Clades A, B, and G. *Cell* **165,** 813–826 (2016).
95. Diskin, R. *et al.* Restricting HIV-1 pathways for escape using rationally

designed anti–HIV-1 antibodies. *J Exp Med* **210,** 1235–1249 (2013).
96. Diskin, R. *et al.* Increasing the potency and breadth of an HIV antibody by using structure-based rational design. *Science* **334,** 1289–1293 (2011).
97. Zhou, T. *et al.* Structural Basis for Broad and Potent Neutralization of HIV-1 by Antibody VRC01. *Science* **329,** 811–817 (2010).
98. Zhou, T. *et al.* Multidonor Analysis Reveals Structural Elements, Genetic Determinants, and Maturation Pathway for HIV-1 Neutralization by VRC01-Class Antibodies. *Immunity* **39,** 245–258 (2013).
99. Zhou, T. *et al.* Structural Repertoire of HIV-1-Neutralizing Antibodies Targeting the CD4 Supersite in 14 Donors. *Cell* **161,** 1280–1292 (2015).
100. Jardine, J. *et al.* Rational HIV immunogen design to target specific germline B cell receptors. *Science* **340,** 711–716 (2013).
101. Tiller, T., Busse, C. E. & Wardemann, H. Cloning and expression of murine Ig genes from single B cells. *Journal of Immunological Methods* **350,** 183–193 (2009).
102. Boehmer, von, L. *et al.* Sequencing and cloning of antigen-specific antibodies from mouse memory B cells. *Nat Protoc* **11,** 1908–1923 (2016).
103. Hoot, S. *et al.* Recombinant HIV Envelope Proteins Fail to Engage Germline Versions of Anti-CD4bs bNAbs. *PLoS Pathog* **9,** e1003106–14 (2013).
104. McGuire, A. T. *et al.* Engineering HIV envelope protein to activate germline B cell receptors of broadly neutralizing anti-CD4 binding site antibodies. *J Exp Med* **210,** 655–663 (2013).
105. Xiao, X. *et al.* Germline-like predecessors of broadly neutralizing antibodies lack measurable binding to HIV-1 envelope glycoproteins: Implications for evasion of immune responses and design of vaccine immunogens. *Biochemical and Biophysical Research Communications* **390,** 404–409 (2009).
106. McGuire, A. T. *et al.* HIV antibodies. Antigen modification regulates competition of broad and narrow neutralizing HIV antibodies. *Science* **346,** 1380–1383 (2014).
107. Sanders, R. W. *et al.* A Next-Generation Cleaved, Soluble HIV-1 Env Trimer, BG505 SOSIP.664 gp140, Expresses Multiple Epitopes for Broadly Neutralizing but Not Non-Neutralizing Antibodies. *PLoS Pathog* **9,** e1003618–20 (2013).
108. Yang, X. *et al.* Highly Stable Trimers Formed by Human Immunodeficiency Virus Type 1 Envelope Glycoproteins Fused with the Trimeric Motif of T4 Bacteriophage Fibritin. *Journal of Virology* **76,** 4634–4642 (2002).
109. Dey, B. *et al.* Structure-Based Stabilization of HIV-1 gp120 Enhances Humoral Immune Responses to the Induced Co-Receptor Binding Site. *PLoS Pathog* **5,** e1000445–15 (2009).

110. Li, M. *et al.* Human Immunodeficiency Virus Type 1 env Clones from Acute and Early Subtype B Infections for Standardized Assessments of Vaccine-Elicited Neutralizing Antibodies. *Journal of Virology* **79,** 10108–10125 (2005).
111. Kwong, P. D. *et al.* Structure of an HIV gp120 envelope glycoprotein in complex with the CD4 receptor and a neutralizing human antibody. *Nature* **393,** 648–659 (1998).
112. Lasky, L. A. *et al.* Neutralization of the AIDS retrovirus by antibodies to a recombinant envelope glycoprotein. *Science* **233,** 209–212 (1986).
113. Julien, J.-P. *et al.* Crystal structure of a soluble cleaved HIV-1 envelope trimer. *Science* **342,** 1477–1483 (2013).
114. Pancera, M. *et al.* Structure and immune recognition of trimeric pre-fusion HIV-1 Env. *Nature* **514,** 455–461 (2014).
115. Garces, F. *et al.* Affinity Maturation of a Potent Family of HIV Antibodies Is Primarily Focused on Accommodating or Avoiding Glycans. *Immunity* **43,** 1053–1063 (2015).
116. Lee, J. H., Ozorowski, G. & Ward, A. B. Cryo-EM structure of a native, fully glycosylated, cleaved HIV-1 envelope trimer. *Science* **351,** 1043–1048 (2016).
117. Doores, K. J. The HIV glycan shield as a target for broadly neutralizing antibodies. *FEBS J.* **282,** 4679–4691 (2015).
118. Behrens, A.-J. *et al.* Composition and Antigenic Effects of Individual Glycan Sites of a Trimeric HIV-1 Envelope Glycoprotein. *CellReports* **14,** 2695–2706 (2016).
119. Binley, J. M. *et al.* Role of Complex Carbohydrates in Human Immunodeficiency Virus Type 1 Infection and Resistance to Antibody Neutralization. *Journal of Virology* **84,** 5637–5655 (2010).
120. Go, E. P. *et al.* Characterization of Glycosylation Profiles of HIV-1 Transmitted/Founder Envelopes by Mass Spectrometry. *Journal of Virology* **85,** 8270–8284 (2011).
121. Gristick, H. B. *et al.* Natively glycosylated HIV-1 Env structure reveals new mode for antibody recognition of the CD4-binding site. *Nat. Struct. Mol. Biol.* **23,** 906–915 (2016).
122. North, B., Lehmann, A. & Dunbrack, R. L., Jr. A New Clustering of Antibody CDR Loop Conformations. *Journal of Molecular Biology* **406,** 228–256 (2011).
123. Adolf-Bryfogle, J., Xu, Q., North, B., Lehmann, A. & Dunbrack, R. L. PyIgClassify: a database of antibody CDR structural classifications. *Nucleic Acids Research* **43,** D432–D438 (2015).
124. McLellan, J. S. *et al.* Structure of HIV-1 gp120 V1/V2 domain with broadly neutralizing antibody PG9. *Nature* **480,** 336–343 (2011).
125. Pancera, M. *et al.* Structural basis for diverse N-glycan recognition by HIV-1–neutralizing V1–V2–directed antibody PG16. *Nat. Struct. Mol. Biol.* **20,** 804–813 (2013).
126. Lyumkis, D. *et al.* Cryo-EM structure of a fully glycosylated soluble cleaved HIV-1 envelope trimer. *Science* **342,** 1484–1490 (2013).

127. West, A. P., Jr *et al.* Structural Insights on the Role of Antibodies in HIV-1 Vaccine and Therapy. *Cell* **156,** 633–648 (2014).
128. Betz, A. G., Neuberger, M. S. & Milstein, C. Discriminating intrinsic and antigen-selected mutational hotspots in immunoglobulin V genes. *Immunol. Today* **14,** 405–411 (1993).
129. Longerich, S., Basu, U., Alt, F. & Storb, U. AID in somatic hypermutation and class switch recombination. *Current Opinion in Immunology* **18,** 164–174 (2006).
130. Neuberger, M. S. *et al.* Monitoring and interpreting the intrinsic features of somatic hypermutation. *Immunol Rev* **162,** 107–116 (1998).
131. Jardine, J. G. *et al.* HIV-1 VACCINES. Priming a broadly neutralizing antibody response to HIV-1 using a germline-targeting immunogen. *Science* **349,** 156–161 (2015).
132. Mouquet, H. *et al.* Complex-type N-glycan recognition by potent broadly neutralizing HIV antibodies. *Proc. Natl. Acad. Sci. U.S.A.* **109,** E3268–77 (2012).
133. Escolano, A. *et al.* Sequential Immunization Elicits Broadly Neutralizing Anti-HIV-1 Antibodies in Ig Knockin Mice. *Cell* **166,** 1445–1458.e12 (2016).
134. Steichen, J. M. *et al.* HIV Vaccine Design to Target Germline Precursors of Glycan-Dependent Broadly Neutralizing Antibodies. *Immunity* **45,** 483–496 (2016).
135. DeKosky, B. J. *et al.* In-depth determination and analysis of the human paired heavy- and light-chain antibody repertoire. *Nat. Med.* **21,** 86–91 (2014).
136. Lee, E.-C. *et al.* Complete humanization of the mouse immunoglobulin loci enables efficient therapeutic antibody discovery. *Nat Biotechnol* **32,** 356–363 (2014).
137. Sok, D. *et al.* Priming HIV-1 broadly neutralizing antibody precursors in human Ig loci transgenic mice. *Science* **353,** 1557–1560 (2016).
138. Jardine, J. G. *et al.* HIV-1 broadly neutralizing antibody precursor B cells revealed by germline-targeting immunogen. *Science* **351,** 1458–1463 (2016).
139. Chung, N. P. Y. *et al.* Stable 293 T and CHO cell lines expressing cleaved, stable HIV-1 envelope glycoprotein trimers for structural and vaccine studies. *Retrovirology* **11,** 33 (2014).
140. Pugach, P. *et al.* A Native-Like SOSIP.664 Trimer Based on an HIV-1 Subtype B envGene. *Journal of Virology* **89,** 3380–3395 (2015).
141. Forsell, M. N. E. *et al.* B Cell Recognition of the Conserved HIV-1 Co-Receptor Binding Site Is Altered by Endogenous Primate CD4. *PLoS Pathog* **4,** e1000171–12 (2008).
142. Sheskin, D. *Handbook of Parametric and Nonparametric Statistical Procedures*. 1–25 (Chapman & Hall/CRC, 2017).
143. Tiller, T. *et al.* Efficient generation of monoclonal antibodies from single human B cells by single cell RT-PCR and expression vector cloning. *Journal of Immunological Methods* **329,** 112–124 (2008).

144. Leaver-Fay, A., Jacak, R., Stranges, P. B. & Kuhlman, B. A generic program for multistate protein design. *PLoS ONE* **6,** e20937 (2011).
145. Galimidi, R. P. *et al.* Intra-Spike Crosslinking Overcomes Antibody Evasion by HIV-1. *Cell* **160,** 433–446 (2015).
146. Jaroszewski, L., Li, Z., Cai, X. H., Weber, C. & Godzik, A. FFAS server: novel features and applications. *Nucleic Acids Research* **39,** W38–W44 (2011).
147. Adams, P. D. *et al.* PHENIX: a comprehensive Python-based system for macromolecular structure solution. *Acta Crystallogr D Biol Crystallogr* **66,** 213–221 (2010).
148. Agirre, J. *et al.* Privateer: software for the conformational validation of carbohydrate structures. *Nat. Struct. Mol. Biol.* **22,** 833–834 (2015).
149. Pettersen, E. F. *et al.* UCSF Chimera?A visualization system for exploratory research and analysis. *J. Comput. Chem.* **25,** 1605–1612 (2004).
150. Collaborative Computational Project Number 4. The CCP4 suite: programs for protein crystallography. *Acta Crystallogr D Biol Crystallogr* **50,** 760–763 (1994).
151. Sievers, F. *et al.* Fast, scalable generation of high-quality protein multiple sequence alignments using Clustal Omega. *Molecular Systems Biology* **7,** 539–539 (2011).